Elastic and inelastic pion-nucleon scattering to fourth order in chiral perturbation theory

D. Siemens, V. Bernard, E. Epelbaum, A. M. Gasparyan, H. Krebs, and Ulf-G. Meißner

Elastic and inelastic pion-nucleon scattering to fourth order in chiral perturbation theory

D. Siemens,[1, *] V. Bernard,[2, †] E. Epelbaum,[1, ‡]
A. M. Gasparyan,[1, 3, §] H. Krebs,[1, ¶] and Ulf-G. Meißner[4, 5, 6, **]

1 Institut für Theoretische Physik II,
Ruhr-Universität Bochum, D-44780 Bochum, Germany
2 Groupe de Physique Théorique, Institut de Physique Nucléaire,
UMR 8608, CNRS, Univ. Paris-Sud,
Université Paris Saclay, F-91406 Orsay Cedex, France
3 Institute for Theoretical and Experimental Physics,
B. Cheremushkinskaya 25, 117218 Moscow, Russia
4 Helmholtz-Institut für Strahlen- und Kernphysik and Bethe Center for Theoretical Physics,
Universität Bonn, D–53115 Bonn, Germany
5 Institute for Advanced Simulation,
Institut für Kernphysik and Jülich Center for Hadron Physics,
Forschungszentrum Jülich, D-52425 Jülich, Germany
6 JARA - High Performance Computing,
Forschungszentrum Jülich, D-52425 Jülich, Germany

Abstract

We extend our previous study of elastic pion-nucleon scattering in the framework of chiral perturbation theory by performing a combined analysis of the reactions $\pi N \to \pi N$ and $\pi N \to \pi\pi N$. The calculation is carried out to fourth order in the chiral expansion using the heavy baryon approach and the covariant formulation supplemented with a modified version of the extended on-mass-shell renormalization scheme. We demonstrate that a combined fit to experimental data in both channels leads to a reduced amount of correlations between the low-energy constants. A satisfactory description of the experimental data in both channels is obtained, which is further improved upon including tree-level contributions of the $\Delta(1232)$ resonance. We also explore a possibility of using the empirical information about πN subthreshold parameters obtained recently by means of the Roy-Steiner equations to stabilize the fits.

* dmitrij.siemens@rub.de

† bernard@ipno.in2p3.fr

‡ evgeny.epelbaum@rub.de

§ ashot.gasparyan@rub.de

¶ hermann.krebs@rub.de

** meissner@hiskp.uni-bonn.de

I. INTRODUCTION

In recent years, there has been a revival of interest in theoretical studies of elastic pion-nucleon scattering. One important milestone is a new partial-wave analysis in the framework of the Roy-Steiner equations [1, 2], which incorporates the fundamental principles of analyticity, crossing symmetry and unitarity. Using the empirical information about high-energy πN and $\pi\pi$ scattering, the authors of Ref. [2] have performed error propagation of all input quantities to finally determine pion-nucleon S- and P-wave phase shifts with quantified uncertainties, see the review [3] for more details.

Considerable progress has also been made toward the understanding of elastic pion-nucleon scattering in the framework of chiral perturbation theory (χPT), an effective field theory of the strong interactions that allows one to perform a systematic expansion of low-energy hadronic observables in powers of the soft scales such as the pion mass M_π and/or external three-momenta of the interacting particles $\boldsymbol{p}_i$. Here and in what follows, we restrict ourselves to the two-flavor case of the light up- and down-quarks. Throughout, we work in the isospin limit $m_u = m_d$. In the single-nucleon sector, special care is required to maintain the chiral power counting in the presence of the nucleon mass m_N. This can be achieved using the heavy-baryon scheme or, alternatively, by exploiting the freedom in the choice of renormalization conditions in the covariant framework.

In the heavy-baryon approach, one performs a $1/m_N$ expansion at the level of the effective Lagrangian [4, 5]. As a result, the nucleon mass only enters the heavy-baryon Lagrangian in the form of $1/m_N$-corrections to the vertices so that no positive powers of m_N can emerge when calculating the corresponding Feynman diagrams. In the single-nucleon sector, the nucleon mass is counted as a quantity of the order of the breakdown scale of the chiral expansion Λ_b, i.e. $m_N \sim \Lambda_b$. Here and in what follows, we denote the resulting approach as HB-πN. In contrast, in few-nucleon calculations one usually treats the nucleon mass as an even larger scale via the assignment $m_N \sim \Lambda_b^2/M_\pi$ [6, 7]. This approach, which we refer to as HB-NN, leads to a stronger suppression of relativistic corrections as compared to the HB-πN scheme. Note that in all our estimates we adopt the conservative value of $\Lambda_b \sim 600$ MeV as in Ref. [8].

For a covariant formulation of baryon χPT, the chiral power counting can be maintained employing the so-called infrared renormalization scheme [9, 10] or, alternatively, by using the extended on-mass-shell scheme (EOMS) [11, 12]. Here and in what follows, we will employ the EOMS approach in a slightly different form as compared with its original formulation. In particular, we require the $1/m_N$-expansion of our results to match exactly the heavy-baryon expansion which can be achieved via performing additional finite renormalization of the low-energy constants (LECs), see Ref. [8] for details.

In Ref. [8], we have studied elastic pion-nucleon scattering to fourth order in the chiral expansion within both the HB and covariant formulations. Differently to the previous χPT studies of this reaction [5, 13–22], we have directly used the available experimental data taken from the GWU-SAID data base [23] rather than the partial wave analyses such as e.g. the ones performed by the Karlsruhe-Helsinki [24] and GWU (SAID) [25] groups to determine the values of the various LECs, see also Ref. [26] for a recent work following the same strategy (where only the HB-NN version of χPT was considered and no theoretical errors were taken into account). In addition, we have carried out a detailed estimation of theoretical uncertainties from the truncation of the chiral expansion by employing the algorithm formulated in Ref. [27]. These two features have allowed us to directly translate the

experimental errors into the statistical uncertainties of the extracted LECs and correlations among them. The predicted phase shifts were found to be in good agreement with the ones of Ref. [2]. Finally, elastic pion-nucleon scattering has also been analyzed at the leading one-loop order in a covariant formulation of χPT with explicit Δ-resonance degrees of freedom [28]. In that work, the LECs have been determined from fits to phase shifts determined in the Roy-Steiner equation analysis of Ref. [2].

There is a fair number of unknown LECs that need to be determined from the fit, namely 8 (13) LECs at order Q^3 (Q^4) with $Q \in \{|\boldsymbol{p}_i|/\Lambda_b,\ M_\pi/\Lambda_b\}$ denoting the expansion parameter in χPT. This results in sizeable uncertainties and large correlations among some of the LECs. It is, therefore, desirable to incorporate additional empirical information when doing the fits in order to further constrain the values of the LECs. χPT provides a suitable tool to achieve this goal as it allows one to apply the same effective Lagrangian to different processes and kinematical regions as long as one stays within the applicability domain of the chiral expansion.

In the present study we explore two possibilities for further constraining the fits. First, we employ the information on the so-called subthreshold πN parameters, which have been extracted recently with high accuracy by means of the Roy-Steiner equation [3]. Secondly, we perform combined fits of the experimental data in elastic pion-nucleon scattering and the inelastic reaction $\pi N \to \pi\pi N$. The corresponding scattering amplitude has been calculated up to the leading one-loop order (i.e. Q^3) in HB formulation of χPT in Refs. [29, 30], see Refs. [31–33] for related earlier studies. Furthermore, single pion production off nucleons was also analyzed at tree level in the covariant χPT framework with an implicit [34] and explicit [35] treatment of effects due to Δ-resonance. A covariant tree-level investigation including both the Δ and the Roper resonances was presented in Ref. [36]. In this work, we extend these calculations by performing, for the first time, a complete analysis of the reaction $\pi N \to \pi\pi N$ at the full one-loop order (i.e. Q^4) using both the HB and covariant formulations of χPT.

Our paper is organized as follows. In section II, we give the definition of the pion-nucleon subthreshold coefficients while section III contains the basic definitions and formalism for the reaction $\pi N \to \pi\pi N$. The details of the fitting procedure can be found in section IV. The discussion of the naturalness of the extracted low-energy constants is presented in section V, where we also discuss the lowest-order contributions of the Δ- and Roper-resonances to these LECs. Our predictions for various observables are collected in section VI, where we also discuss the obtained results. Finally, the main results of our study are summarized in section VII. The appendix contains explicit expressions for the resonance saturation of LECs due to the explicit inclusion of lowest-order $\Delta(1232)$- and Roper-resonance.

II.   PION-NUCLEON SUBTHRESHOLD PARAMETERS

As already pointed out in the introduction, this work provides an extension of the previous analysis of the reaction $\pi N \to \pi N$ in [8]. In particular, we explore the possibility to improve the extraction of the πN LECs by incorporating additional constraints from the subthreshold kinematical region by including the leading subthreshold parameters in our fitting procedure. In the following, we provide the basic definitions of the subthreshold parameters. A detailed discussion of our calculation of the πN scattering amplitude including the definitions of observables and kinematics as well as the details concerning renormalization up to order Q^4 can be found in Ref. [8].

The T-matrix for the process $\pi^a(q)\,N(p) \;\to\; \pi^b(q')\,N'(p')$ can be conveniently expressed in the form

$$T^{ba} = \chi_{N'}^{\dagger}\left(\delta^{ab}T^+ + \mathrm{i}\epsilon^{bac}\tau_c T^-\right)\chi_N \;, \qquad T^{\pm} \;= \bar{u}^{(s')}\left(D^{\pm} - \frac{1}{4m_N}[\not{q}',\not{q}]B^{\pm}\right)u^{(s)}\;, \qquad (1)$$

where the amplitudes $D^{\pm}$ and $B^{\pm}$ depend on the quantities t and $\nu = (s-u)/4m_N$, with the Mandelstam variables defined as

$$s = (p+q)^2\;, \quad t = (q-q')^2\;, \quad u = (p'-q)^2\;, \quad s+t+u = 2m_N^2 + 2M_\pi^2\;. \qquad (2)$$

The subthreshold parameters are defined by an expansion of the amplitudes in powers of ν and t via [18, 37]

$$D^{\pm} = \binom{1}{\nu}\sum_{n,m=0}^{\infty} d_{mn}\nu^{2m}t^n + D^{\pm}_{\mathrm{pv}}\;, \quad B^{\pm} = \binom{\nu}{1}\sum_{n,m=0}^{\infty} b_{mn}\nu^{2m}t^n + B^{\pm}_{\mathrm{pv}}\;, \qquad (3)$$

where $B^{\pm}_{\mathrm{pv}}$ and $D^{\pm}_{\mathrm{pv}}$ refer to the subtracted pseudovector Born-term contributions given by

$$B^{\pm}_{\mathrm{pv}} = g_{\pi NN}^2\left(\frac{1}{m_N^2-s}\mp\frac{1}{m_N^2-u}\right) - \frac{g_{\pi NN}^2}{2m_N^2}\binom{0}{1}\;, \quad D^{\pm}_{\mathrm{pv}} = \frac{g_{\pi NN}^2}{m_N}\binom{0}{1} + \nu B^{\pm}_{\mathrm{pv}}\;. \qquad (4)$$

III.   THE REACTION $\pi N \to \pi\pi N$

We now turn to the reaction $\pi N \to \pi\pi N$ and mainly focus on the renormalization of the amplitude. To be more precise, we follow the same procedure as for the elastic channel in Ref. [8] and only present in the following the new features appearing in the pion production process. More details on the studied observables, in particular the relations to the amplitude, can be found in Ref. [35].

The T-matrix for the reaction $\pi^a(q_1)\,N(p) \;\to\; \pi^b(q_2)\,\pi^c(q_3)\,N'(p')$ can be expressed in terms of four invariant amplitudes

$$T^{abc} = \mathrm{i}\bar{u}^{(s')}\gamma_5\left(F_1^{abc} + (\not{q}_2+\not{q}_3)\tilde{F}_2^{abc} + (\not{q}_2-\not{q}_3)\tilde{F}_3^{abc} + \not{q}_1(\not{q}_2\not{q}_3 - \not{q}_3\not{q}_2)\tilde{F}_4^{abc}\right)u^{(s)}\;, \qquad (5)$$

which depend on the five Mandelstam variables

$$s = (p+q_1)^2\;, \quad s_1 = (q_2+p')^2\;, \quad s_2 = (q_3+p')^2\;, \quad t_1 = (q_2-q_1)^2\;, \quad t_2 = (q_3-q_1)^2\;. \qquad (6)$$

Notice that in Ref. [35], a different basis was chosen to decompose the amplitude. The amplitudes $\tilde{F}_i^{abc}$ are related to the ones F_i^{abc} used in Ref. [35] via

$$\begin{aligned}
\tilde{F}_1 &= F_1\;,\\
\tilde{F}_2 &= F_2 - \frac{1}{2m_N}(s_1 - s_2 + t_1 - t_2)F_4\;,\\
\tilde{F}_3 &= F_3 - \frac{1}{2m_N}(4M_\pi^2 + m_N^2 - s - t_1 - t_2)F_4\;,\\
\tilde{F}_4 &= -\frac{1}{2m_N}F_4\;.
\end{aligned} \qquad (7)$$

The isospin decomposition of the invariant amplitudes reads

$$F_i^{abc} = \chi_{N'}^\dagger \left(\tau^a \delta^{bc} B_i^1 + \tau^b \delta^{ac} B_i^2 + \tau^c \delta^{ab} B_i^3 + \mathrm{i}\epsilon^{abc} B_i^4 \right) \chi_N. \tag{8}$$

The basis in Eq. (5) is better suited for the renormalization procedure, because each spin structure fulfills the power-counting on its own. Like in the case of πN-scattering, the individual spin structures are expanded in small parameters,

$$M_\pi \sim \mathcal{O}(Q^1), \quad s - m_N^2 \sim \mathcal{O}(Q^1), \quad s_1 - m_N^2 \sim \mathcal{O}(Q^1), \quad s_2 - m_N^2 \sim \mathcal{O}(Q^1),$$
$$t \sim \mathcal{O}(Q^2), \quad t_1 \sim \mathcal{O}(Q^2), \quad t_2 \sim \mathcal{O}(Q^2), \tag{9}$$

which allows one to identify the power-counting breaking terms. The linear combination $s - s_1 - s_2 + m_N^2$ counts, according to the above rules, as a quantity of order Q^1 but actually starts contributing at order Q^2. It is, therefore, advantageous to express the invariant amplitudes as functions of e.g. s_1, s_2, t, t_1 and t_2. In the following, all LECs should be understood as renormalized quantities and the explicit shifts used for the renormalization can be found in Ref. [8].

The relevant tree-level diagrams for the reaction $\pi N \to \pi\pi N$ to order Q^4 are shown in Fig. 1 while the leading-order loop diagrams at order Q^3 are visualized in Figs. 2 and 3. The subleading one-loop diagrams at order Q^4 are not shown explicitly, but can be easily generated by replacing each leading-order vertex with an even number of pions from the Lagrangian $\mathcal{L}_{\pi N}^{(1)}$ with a subleading one from $\mathcal{L}_{\pi N}^{(2)}$ as visualized in Fig. 4. Notice that there are no vertices with an odd number of pions in the Lagrangian $\mathcal{L}_{\pi N}^{(2)}$. We also do not show here the Feynman diagrams contributing to πN-scattering, which can be easily identified by observing that $\pi N \to \pi N$ is a subprocess of $\pi N \to \pi\pi N$ (see Fig. 5), see also Ref. [17].

The leading-order tree-level diagrams are constructed solely from the lowest-order vertices and thus depend only on the well-known LECs F_π and g_A. The higher-order tree-level graphs involve insertions of the LECs c_i from $\mathcal{L}_{\pi N}^{(2)}$, d_i from $\mathcal{L}_{\pi N}^{(3)}$, e_i from $\mathcal{L}_{\pi N}^{(4)}$ and the purely mesonic LECs l_i from $\mathcal{L}_{\pi\pi}^{(4)}$, which are known from $\pi\pi$-scattering and other pion observables. Specifically, the πN-scattering amplitudes depend on the LECs $c_{1,2,3,4}$, $d_{1+2,3,5,14-15}$ and $e_{14,15,16,17,18}$. These LECs also enter the $\pi N \to \pi\pi N$ amplitudes. Notice that due to crossing symmetry, the contributions proportional to the LECs $e_{14,15,16}$ count as order-Q^5 and for this reason are set to zero. Finally, the $\pi N \to \pi\pi N$ scattering amplitude depends on additional LECs accompanying the πN-vertices with three pions, namely $d_{4,10,11,12,13,16,18}$ from $\mathcal{L}_{\pi N}^{(3)}$ and $e_{10,11,12,13,34}$ from $\mathcal{L}_{\pi N}^{(4)}$. Note that the LECs d_4 and $e_{11,12,13,34}$ only contribute to the channels $\pi^+ p \to \pi^+\pi^0 p$ and $\pi^- p \to \pi^0\pi^- p$. The other LECs contribute to all channels. Finally, we neglect the contributions proportional to the LEC e_{35}, which appear in the amplitudes of both reactions since the corresponding terms actually count as order-Q^5.

IV. FIT PROCEDURE

The amplitudes for the reactions $\pi N \to \pi N$ and $\pi N \to \pi\pi N$ depend on several LECs as explained in the previous section. To extract the LECs c_i, d_i and e_i from the data, we follow the same fit procedure to the available pion-nucleon scattering data up to $T < 100$ MeV as in Ref. [8] but employ two kinds of additional constraints as discussed below.

5

A. Constraints from subthreshold parameters

As a first approach, we consider elastic pion-nucleon scattering but, differently to our previous study in Ref. [8], include in the fitting procedure additional constraints from the subthreshold region. Specifically, we minimize the quantity

$$\chi^2 = \chi^2_{\pi N} + \chi^2_{\text{RS}} , \tag{10}$$

where $\chi^2_{\pi N}$ is the standard sum of squares

$$\chi^2_{\pi N} = \sum_i \left(\frac{\mathcal{O}_i^{exp} - N_i \mathcal{O}_i^{(n)}}{\delta \mathcal{O}_i} \right)^2 \qquad \text{with} \qquad \delta \mathcal{O}_i = \sqrt{(\delta \mathcal{O}_i^{exp})^2 + (\delta \mathcal{O}_i^{(n)})^2} . \tag{11}$$

The experimental data $\mathcal{O}_i^{exp}$, experimental errors $\delta \mathcal{O}_i^{exp}$ and normalization factors N_i are taken from the GWU-SAID data base [23]. The quantity $\mathcal{O}_i^{(n)}$ labels the corresponding observable calculated to chiral order n, whereas the theoretical error $\delta \mathcal{O}_i^{(n)}$ is based on the truncation of the chiral expansion [8, 27]. In addition, the quantity χ^2_{RS} is defined in analogy to Eq. (11) as the standard sum of squares, which includes the eight leading πN scattering subthreshold parameters given by the Roy-Steiner analysis [3], namely $d_{00}^\pm$, $d_{10}^\pm$, $d_{01}^\pm$ and $b_{00}^\pm$. The Roy-Steiner analysis uses as an input data on the t-channel reactions (corresponding to the $\pi\pi$, $\bar{K}K$, $\bar{N}N$ and other channels), the πN scattering lengths obtained from the analysis of pionic atoms, the values of the πN S- and P-wave phase shifts at higher energies, and the values of the πN phase shifts for higher partial waves. Implementing the principles of analyticity and unitarity the πN scattering amplitude is continued to the subthreshold region. Therefore, the subthreshold parameters obtained this way contain complementary information to the low-energy πN data. Among the above-mentioned sources of input information only the πN phase shifts for higher partial waves could cause some small amount of double counting of near-threshold data. The weights in both sums of squares in Eq. (10) include the experimental error as well as an estimated theoretical error based on the truncation of the chiral series. The interested reader is referred to Ref. [8] for more details on the fitting procedure. Notice that we choose the values of the LECs determined by the subthreshold coefficients alone, see Ref. [38], as a starting point in our iterative fitting procedure. However, we checked that the final minimum is independent of the starting point.

One should mention here that adding a theoretical uncertainty in quadrature as in Eq. (11) is an approximation because of correlations of theoretical errors at different data points (see e.g. Refs. [39, 40]). We will also make use of the quantity

$$\bar{\chi}^2_{\pi N} = \sum_i \left(\frac{\mathcal{O}_i^{exp} - N_i \mathcal{O}_i^{(n)}}{\delta \mathcal{O}_i^{exp}} \right)^2 , \tag{12}$$

where theoretical errors are not taken into account.

The extracted values of the LECs at orders Q^2, Q^3, Q^4 are listed in Table I for the heavy-baryon and covariant schemes along with the corresponding values of the reduced $\chi^2_{\pi N}$ ($\bar{\chi}^2_{\pi N}$) with (without) theoretical error. For the sake of compactness, we restrict ourselves, following Ref. [8], to the fits with $T_\pi < 100$ MeV that correspond to 1704 πN experimental data points. The number of degrees of freedom (dof) is equal to the number of data points minus the number of fitted parameters. Note that the relative weight of the χ^2_{RS} in the total minimal

6

χ^2, e.g. for the fits at order Q^4, does not exceed 2%. Nevertheless, due to small uncertainties of the subthreshold parameters given by the Roy-Steiner analysis (typically of the order of a few percent), it's statistical importance is sufficient to influence the fit. To have a simpler comparison, we also show the values of the LECs extracted in Ref. [8] and the corresponding reduced $\chi^2_{\pi N}$ ($\bar{\chi}^2_{\pi N}$).

As can be seen from Table I, imposing constraints from subthreshold parameters does not lead to a qualitative improvement of the statistical uncertainties in the determination of the LECs. However, strong correlations present in the pure πN fit (see Ref. [8]) are weakened. In a combined fit, no correlation coefficient among the LECs exceeds (by absolute value) 0.9. Instead of showing the full covariance/correlation matrix, we prefer to only discuss the strongly correlated LECs in the pure πN fit (at highest considered order–Q^4). In particular, in the HB-NN counting scheme one observes strong (anti-)correlations between c_1 and c_2 (0.90), between c_2 and e_{16} (−0.94) and between c_2 and d_{1+2} (0.94), which in the fits including the constraints from the subthreshold region are reduced to (0.73), (−0.62) and (0.87), respectively. In the HB-πN scheme, one has a similar situation regarding correlations between the same set of LECs, which are reduced from (0.93), (−0.93) and (0.94) to (0.86), (−0.59) and (0.88), respectively. In the covariant approach, one only has a strong correlation between c_1 and c_2 (0.92), which is reduced to (0.81). The inclusion of the information about the subthreshold coefficients in the fits could result in deteriorating the description of the pion-nucleon scattering data in the physical region. By comparing the corresponding $\bar{\chi}^2_{\pi N}$ values listed in Table I at order Q^4, we indeed observe this to be the case in the HB-πN approach.[1] This can be viewed as an indication that the HB χPT fails to provide simultaneous description of the pion-nucleon scattering amplitude both in the physical and subthreshold regions which is consistent with the findings of Refs. [8, 38, 41]. The smallest change in $\bar{\chi}^2_{\pi N}$ and in the values of the LECs upon including the information about the subthreshold coefficients in the fit is observed in the covariant approach. This should not come as a surprise given the superior description of the subthreshold coefficients based on the LECs determined from πN scattering data alone in this formulation.

B. Constraints from the reaction $\pi N \to \pi\pi N$

In the second approach, we include additional constraints from the reaction $\pi N \to \pi\pi N$ such that we minimize

$$\chi^2 = \chi^2_{\pi N} + \chi^2_{\pi\pi N} + \chi^2_{\pi\pi} , \qquad (13)$$

where $\chi^2_{\pi N}$ is defined as in Eq. (11), $\chi^2_{\pi\pi N}$ is defined analogously and includes the pion-production total cross section data up to the maximal energy of $T_\pi < 350$ MeV as well as double differential cross section data at $T_\pi = 200$ MeV and $T_\pi = 230$ MeV. The total cross sections are taken from the compilation [42] and from [43], [44] and [45], whereas the double-differential cross sections with respect to Ω_2 and the pion kinetic energy $T_2 = \omega_2 - M_\pi$ in the channel $\pi^- p \to \pi^+ \pi^- n$ are reported in [46]. The information about $\pi\pi$ scattering data is included indirectly in $\chi^2_{\pi\pi}$ by using the extracted LECs l_i including uncertainties as a sum

---

[1] It is more difficult to interpret the results at lower orders due to the dependence of the employed theoretical uncertainties on the fit results at subsequent chiral orders as explained in detail in [8].

of squares

$$\chi^2_{\pi\pi} = \sum_i^4 \left(\frac{l_i - \bar{l}_i}{\Delta \bar{l}_i} \right)^2 , \qquad (14)$$

where we used the values for the relevant LECs from $\mathcal{L}^{(4)}_{\pi\pi}$ summarized in [47] [2]

$$\bar{l}_1 = -0.4 \pm 0.6 , \quad \bar{l}_2 = 4.3 \pm 0.1 , \quad \bar{l}_3 = 2.9 \pm 2.4 , \quad \bar{l}_4 = 4.4 \pm 0.2 . \qquad (15)$$

Note that $\Delta \bar{l}_i$ denotes the statistical error such that we do not employ a theoretical error in $\chi^2_{\pi\pi}$.

As was seen in the analysis of [8], the Δ pole at $T_\pi \simeq 190$ MeV and the strong coupling of the Δ to the πN sector prevents one from using elastic pion-nucleon scattering data at energies higher than $T_\pi \sim 100$ MeV when extracting the LECs using Δ-less formulations of χPT. The situation in the reaction $\pi N \to \pi\pi N$ is somewhat different in the sense that the coupling of the Δ to the $\pi\pi N$ sector is very weak as compared to the coupling to the πN sector. This can be seen in the data on decay channels of the Δ [49], where $\Delta \to \pi N$ contributes to $\sim 100\%$, while the channel $\Delta \to \pi\pi N$ is not even listed in Particle Data Group [49]. Also, the observables such as the total cross sections do not show any pronounced structure in the energy region of the Δ pole. Notice further that in the reaction $\gamma N \to \pi\pi N$ at threshold one also expects an overwhelming contribution from the Δ. However, it was shown in Ref. [50] that there are exact cancellations in the single and double-Δ tree graphs at threshold that suppress the dangerous denominator $1/(m_\Delta - m_n - 2M_\pi)$. Thus, it does not appear to be a priori unreasonable to perform fits to $\pi N \to \pi\pi N$ experimental data in the Δ region using deltaless formulations of χPT. It should, however, be emphasized that the reaction $\pi N \to \pi\pi N$ has an additional subdecay channel $\Delta \to \pi N$ (via $\pi N \to \pi\Delta$ channel) for $T_\pi \gtrsim 380$ MeV, which might lead to further limitations on the theory. Moreover, the influence of the Roper resonance may become significant when the energy increases. Although its nominal position corresponds to the laboratory energy of $T_\pi \approx 490$ MeV, the Roper resonance has a rather large width and a fairly strong coupling to the $\pi\pi N$ channel [49]. According to the covariant tree-level study in [36], the Roper indeed plays a visible role in some channels. For other studies of the effects of the Δ and the Roper resonance in the considered energy region, see e.g. Refs. [51, 52].

We performed fits to the discussed $\pi N \to \pi\pi N$ data with incoming pion kinetic energy $T_{\pi,\pi\pi N} < \{250, 275, 300, 325, 350\}$ MeV, which corresponds to $\{87, 101, 122, 132, 140\}$ data points, respectively. Note that the energy range for calculating $\chi^2_{\pi N}$ ($\bar{\chi}^2_{\pi N}$) is always taken to be $T_\pi < 100$ MeV. The fitted LECs as functions of the maximal fitting energy $T_{\pi,\pi\pi N}$ are shown in Figs. 8, 9 and 10 while the reduced $\chi^2_{\pi N}$ ($\bar{\chi}^2_{\pi N}$) and $\chi^2_{\pi\pi N}$ ($\bar{\chi}^2_{\pi\pi N}$) with (without) theoretical errors as a function of $T_{\pi,\pi\pi N}$ is plotted in Fig. 7. Here, the number of degrees of freedom (dof) for the $\pi N \to \pi\pi N$ reaction is defined as the number of the data points for this reaction minus the number of additional parameters not appearing in the πN scattering amplitude. We interpret the stability of the fit against the maximum fitted energy as an indicator of convergence of the chiral expansion in the considered energy region and of the correct choice of the breakdown scale Λ_b (a similar strategy was introduced in Ref. [40]). We do not employ here more sophisticated methods based on the Bayesian approach as it was done e.g. in Refs. [53, 54]. While the fits at Q^3 exhibit a plateau-like behaviour of the

---

[2] A recent compilation of the various results from the lattice simulations can be found in [48].

extracted LECs as well as of the $\chi^2_{\pi N}/\text{dof}$ and $\chi^2_{\pi\pi N}/\text{dof}$ with regard to the maximal energy of the $\pi N \to \pi\pi N$ data, the $\chi^2_{\pi\pi N}/\text{dof}$ and the extracted LECs at Q^4 deviate rather strongly from a constant behaviour when the energy is increased. Optimistically, only the fit results up to 275 MeV may be regarded as reasonably stable. Moreover, as shown in the lowest row of Fig. 7, the description of the $\pi N \to \pi\pi N$ data actually deteriorates at order Q^4 as compared to the order Q^3 except for the results within the covariant approach at energies below 300 MeV. The problem can be traced back to the large values of some of the d_i, which are preferred by the πN scattering data at order Q^4 and seem to be in conflict with the $\pi N \to \pi\pi N$ data. This especially applies to the linear combination d_{14-15}, which changes its value from $d_{14-15} \sim -6$ GeV^{-2} at Q^3 to $d_{14-15} \sim -10$ GeV^{-2} at Q^4 in the covariant approach. We, however, found that the magnitude of the linear combination d_{14-15} at Q^4 has to be much smaller in order to improve the convergence pattern of the chiral expansion in the single-pion production. Notice that the low-energy constants contributing to elastic pion-nucleon scattering are known to become significantly smaller in magnitude upon explicit treatment of the Δ-resonance. This effect of resonance saturation was observed, in particular, in Ref. [8], where the leading-order Δ-contributions have been included. Unfortunately, as will be discussed in section V, the analogous simplified inclusion of the Δ-resonance in the $\pi N \to \pi\pi N$ reaction is less straightforward due to the appearance of a number of additional free parameters. Moreover, as already mentioned above, one cannot a priori exclude the possibility that the Roper-resonance provides significant contributions to some of the $3\pi NN$ LECs as well, while its contribution to the leading $2\pi NN$ LECs $c_{1,2,3,4}$ is known to be marginal [55]. A consistent inclusion of the Δ and Roper resonances in the framework of χPT, which may be needed to increase the applicability range of the theory, is, however, beyond the scope of this paper.

The values of the LECs extracted at orders Q^2, Q^3, Q^4 are collected in Tables II and III for all considered approaches along with the corresponding values of the reduced $\chi^2_{\pi N}$ and $\chi^2_{\pi\pi N}$. To demonstrate the impact of the constraints from the reaction $\pi N \to \pi\pi N$, we restrict ourselves to the fits with $T_{\pi,\pi\pi N} < 275$ MeV where our results are fairly stable.

In general, the change of the LECs as compared to the pure πN fit appears to be small. This can be traced back to the almost complete decoupling of the $\pi N \to \pi\pi N$ component of the χ^2 from the $\pi N \to \pi N$ one caused by the large theoretical uncertainties in the $\pi N \to \pi\pi N$ sector. Also the statistical errors and correlations of the LECs remain almost unchanged. In addition, we observe strong anticorrelations between the LECs d_{10}, d_{12} and d_{11}, d_{13}, see Table IV for the results in the covariant approach.

V. NATURALNESS OF THE LECS

Let us comment on the extracted numerical values of the 3πNN LECs given in Table III. Indeed at first sight they appear to be rather large if we would be using the very naive estimation based on the naturalness assumption,

$$c_i \sim \frac{1}{\Lambda_b} \sim 2\,\text{GeV}^{-1}\,, \qquad d_i \sim \frac{1}{\Lambda_b^2} \sim 3\,\text{GeV}^{-2}\,, \qquad e_i \sim \frac{1}{\Lambda_b^3} \sim 5\,\text{GeV}^{-3}\,, \qquad (16)$$

where $\Lambda_b = 600$ MeV is used to estimate the breakdown scale of the chiral expansion. For the unnaturally large 2πNN LECs, the origin of their enhancement can be traced back to the implicit treatment of the Δ resonance [55]. As shown in [8, 56], the explicit inclusion of the leading Δ-pole diagrams leads to natural values for all LECs. Following the same

strategy, we have repeated the fits including the leading Δ-pole diagrams in the reaction $\pi N \to \pi\pi N$ while setting the additional LECs from the Δ sector to their large-N_c values, namely $h_A = 1.35$ and $g_1 = 2.29$. The results for the 3πNN LECs at order $Q^4 + \delta^1$ are given in Table IV, whereas the 2πNN LECs are not given explicitly but are in very good agreement with the ones determined in [8]. As can be seen from the table, the LECs d_i still remain large whereas the LECs e_i do indeed become more natural as compared to the deltaless fits. Notice further that the statistical errors and the correlations among the LECs $d_{10,11,12,13}$ get enhanced (see Table IV) upon including the δ^1-contributions.

To get further insights into the observed pattern, it is instructive to consider the NLO contributions of the Δ and Roper resonances to the relevant LECs, which are explicitly given in appendix A. These expressions are based on the effective Lagrangian

$$
\begin{aligned}
\mathcal{L}_{\pi\Delta}^{(1)} &= -\bar{\Psi}_i^\mu \Big[(\mathrm{i}\slashed{D}^{ij} - m_\Delta \delta^{ij})g_{\mu\nu} - \mathrm{i}(\gamma_\mu D_\nu^{ij} + \gamma_\nu D_\nu^{ij}) + \mathrm{i}\gamma_\mu \slashed{D}^{ij}\gamma_\nu + m_\Delta \delta^{ij}\gamma_\mu \gamma_\nu \\
&\qquad + \frac{g_1}{2} g_{\mu\nu} \slashed{u}^{ij}\gamma_5 \Big] \Psi_j^\nu \,, \\
\mathcal{L}_{\pi N\Delta}^{(1)} &= h_A\, \bar{\Psi}_\mu^i \Theta^{\mu\alpha}(z_0) w_\alpha^i \Psi + \text{h.c.} \,, \\
\mathcal{L}_{\pi N\Delta}^{(2)} &= \bar{\Psi}_\mu^i \Theta^{\mu\alpha}(z_1) \Big[\frac{b_4}{2} w_\alpha^i w_\beta^j \gamma^\beta \gamma_5 \tau^j + \frac{b_5}{2} w_\alpha^j w_\beta^i \gamma^\beta \gamma_5 \tau^j \Big] \Psi + \text{h.c.} \,, \\
\mathcal{L}_{\pi R}^{(1)} &= \bar{\Psi}_R \Big[\mathrm{i}\slashed{D} - m_R + \frac{g_{RR}}{2}\slashed{u}\gamma_5 \Big] \Psi_R \,, \\
\mathcal{L}_{\pi R}^{(2)} &= \bar{\Psi}_R \Big[c_1^R \langle \chi_+ \rangle + \frac{c_2^R}{8m^2}(-\langle u_\mu u_\nu \rangle D^{\mu\nu} + \text{h.c.}) + \frac{c_3^R}{2}\langle u \cdot u \rangle - \frac{c_4^R}{2}\sigma^{\mu\nu}[u_\mu, u_\nu] \Big] \Psi_R \,, \\
\mathcal{L}_{\pi RN}^{(1)} &= \bar{\Psi}_R \Big[\frac{g_{RN}}{2}\slashed{u}\gamma_5 \Big] \Psi + \text{h.c.} \,, \\
\mathcal{L}_{\pi R\Delta}^{(1)} &= g_{R\Delta}\, \bar{\Psi}_\mu^i \Theta^{\mu\alpha}(z_2) w_\alpha^i \Psi_R + \text{h.c.} \,,
\end{aligned}
\tag{17}
$$

where the Roper contributions are introduced in a close analogy with the pion-nucleon Lagrangian in Ref. [16], as first done in [57] , and the pion-nucleon-Δ Lagrangian is taken from Refs. [58, 59]. Details on the notation used in Eq. (17) can be found in Refs. [16, 35, 58, 59]. Note that we set the off-shell parameters $z_i = 0$ in the explicit expressions. The numerical contributions of the Δ and Roper resonances to the considered LECs are summarized in Table V. The numerical values are obtained by assuming natural values for the unknown LECs entering these expressions. In the Δ-sector, we fix $h_A = 1.35$ and $g_1 = \pm 2.29$ to their large N_C values and employ $b_4 = b_5 = \pm 1$. In the Roper sector, we fix $g_{RN} = 0.35$ as determined by the decay width of $R \to \pi N$ [57] and assume $g_{RR} = g_{R\Delta} = c_i^R = \pm 1$. As can be seen, the contributions to the LECs from the leading-order Δ-pole diagrams employed in our fits ($g_1 = 2.29$) are relatively small for the large LECs $d_{10,11,12,13}$ while quite substantial for the large LECs $e_{10,11,12,13}$. This pattern is consistent with the $Q^4 + \delta^1$ values of the LECs listed in Table IV. Concerning the higher-order contributions, we find some potentially large terms proportional to b_4, b_5 as well as to $g_{R\Delta}$. The remaining contributions of the Roper resonance are rather small and can be neglected. Note that the LECs c_i were redefined to absorb redundant contributions proportional to certain linear combinations of e_i [8], which induces the explicit μ-dependence of c_i even in the HB approach.

Having established that the large values of the 3πNN LECs d_i cannot be explained by means of resonance saturation, it is instructive to address their sensitivity to the choice of the renormalization scale μ. To be specific, we consider the changes in the values of the

LECs by changing the renormalization scale μ from M_π to m_N,

$$\Delta x \equiv x\big|_{\mu=m_N} - x\big|_{\mu=M_\pi}\,, \qquad \overline{\Delta x} = \frac{x(\mu = M_\pi)}{\Delta x}\,, \tag{18}$$

where $x \in \{c_i, d_i, e_i\}$. The quantity Δx gives the absolute change of a LEC x, whereas $\overline{\Delta x}$ is a measure of its relative change. Notice that throughout this work, we follow the convention by choosing $\mu = M_\pi$. The renormalization-group (RG) flow of the LECs is determined by the corresponding dimensionless β-functions. At one-loop level, one finds

$$\Delta x = \frac{\beta_x}{32\pi^2 F_\pi^2} \log\left(\frac{M_\pi^2}{m_N^2}\right)\,, \tag{19}$$

and the β-functions can be found in [8] for both the covariant and heavy-baryon approaches. As can be seen from Table V, the shifts in the 3πNN LECs under the considered change of the renormalization point appear to be much larger than the ones in the 2πNN LECs and are, in most cases, of the same order of magnitude as the LECs themselves. This provides yet another indication that the observed large size of these LECs is not related to the implicit treatment of the Δ and Roper resonances but is rather caused by the corresponding dimensionless β-functions being numerically large. While such enhancement of the β-functions may emerge due to combinatorial reasons such as the products of spin and/or isospin matrices or powers of g_A, which could affect the convergence pattern of the chiral expansion, it could also come from the adopted form of the effective Lagrangian which is a matter of convention. Thus, one cannot a priori exclude the possibility that the large values of the LECs simply reflect the convention employed in the effective Lagrangian. More precisely, the vertices with many pions contain factorial factors that are not reflected in the corresponding terms in the effective Lagrangian. Another interesting observation is that the LECs c_i decrease in magnitude when the renormalization scale is increased, while the LECs d_i show the opposite behaviour and grow in magnitude when increasing the renormalization scale. For the LECs e_i one has a mixed pattern, where the 2πNN LECs increase and the 3πNN LECs decrease in magnitude.

We now further elaborate on the possibility that the large numerical values of the 3πNN LECs are caused by the convention employed in the effective Lagrangian as explained before. Due to the complexity of the $\pi N \to \pi\pi N$ amplitudes involving several energy scales, it is, however, difficult to estimate the contributions from each individual LEC and to identify possible numerical enhancements of this sort. One simple approach is to perform an expansion around the threshold point $\omega_2 = \omega_3 = M_\pi$ and $\boldsymbol{q_1} \cdot \boldsymbol{q_2} = \boldsymbol{q_1} \cdot \boldsymbol{q_3} = \boldsymbol{q_2} \cdot \boldsymbol{q_3} = 0$, such that each Taylor coefficient of that series only involves the scales M_π and m_N. In the following we will consider one representative example. A threshold expansion of the HB-NN amplitude for the channel $\pi^+ p \to \pi^+ \pi^- n$ denoted by III gives

$$T_{III} \simeq \left[-\frac{4\mathrm{i}}{F_\pi^3}\Big(2(d_{10} + d_{12}) + d_{11} + d_{13} + 6g_A(d_{1+2} + d_3 + d_5))\Big)M_\pi^2 + \right.$$
$$\left. + \frac{2\mathrm{i}}{F_\pi^3}\Big(2d_{10} + d_{11} + 3g_A(2d_{1+2} - d_{14-15})\Big)\boldsymbol{q_1} \cdot \boldsymbol{q_3} + \dots \right] S \cdot q_2 + \dots\,, \tag{20}$$

where we only display contributions proportional to the d_i. As can be seen, the contribution from the 3πNN LECs, namely d_{10}, d_{11}, d_{12} and d_{13}, is suppressed by large numerical factors relative to the one of the 2πNN LECs. This is an indication that the large numerical

values of the $3\pi NN$ LECs resulting from our fits merely reflect the chosen normalization in the effective Lagrangian. Also, one should keep in mind that only combinations of these LECs show up. Given that there are some non-negligible correlations between these LECs, looking at the individual values might be misleading. Similar observations can be made for the $3\pi NN$ LECs e_i. All this requires more detailed studies that go beyond the scope of this work. However, we would like to stress that especially in the nucleon sector where multiple powers of the axial coupling constant enter, the usage of the very naive assumption about the natural size of the LECs, Eq. (16) when increasing the order one is working with, should be taken with a grain of salt.

VI.   PREDICTIONS

Based on the LECs extracted in the previous section, we are now in the position to make predictions for various observables. In particular, we focus on the threshold and subthreshold πN coefficients. The relation of the πN amplitude to the subthreshold parameters is given in section II. The threshold expansion of the amplitudes

$$\text{Re}\, D^\pm = \sum_{n,m=0}^\infty D_{mn}^\pm \boldsymbol{q}^{2m} t^n \,, \quad \text{Re}\, B^\pm = \sum_{n,m=0}^\infty B_{mn}^\pm \boldsymbol{q}^{2m} t^n \tag{21}$$

is related to the threshold parameters via the expansion of the partial wave amplitude

$$\text{Re}\, T_{l\pm} = q^{2l+1}(a_{l\pm} + b_{l\pm}\boldsymbol{q}^2 + \dots) \tag{22}$$

such that the parameters of interest are given by

$$a_{0+}^\pm = \frac{D_{00}^\pm}{4\pi(1+\alpha)} \,, \qquad b_{0+}^\pm = -\frac{(2-\alpha)D_{00}^\pm + 8D_{01}^\pm m_N^2\alpha - 4D_{10}m_N^2\alpha - 2B_{00}m_N\alpha^2}{16\pi m_n^2\alpha(1+\alpha)} \,,$$
$$a_{1+}^\pm = -\frac{B_{00}^\pm - 4D_{01}^\pm m_N}{24\pi m_N(1+\alpha)} \,, \qquad a_{1-}^\pm = -\frac{3D_{00}^\pm - 8D_{01}^\pm m_N^2 - B_{00}^\pm m_N(4+6\alpha)}{48\pi m_N^2(1+\alpha)} \,, \tag{23}$$

with $\alpha = M_\pi/m_N$.

Our results for the sub- and threshold parameters based on the different fit approaches are collected in Table VI and VII, respectively. As one would expect, the description of the subthreshold parameters improves when using them as an additional constraint and remains similar in quality to the pure πN fit when performing a combined fit with $\pi N \to \pi\pi N$ reaction. In general, the agreement with the subthreshold and threshold parameters obtained from the Roy-Steiner (RS) equations is better in the covariant approach. This scheme also yields results which are more stable against introducing additional constraints as compared with the HB χPT formulations.

Next, our predictions for the πN phase shifts in S and P partial waves up to pion energies of 100 MeV are given in Figs. 11 and 12 for the two different fit strategies in comparison with the RS results of Ref. [3]. A comparison of Fig. 11 and Fig. 9 of Ref. [8] reveals that the additional constraints from the subthreshold coefficients have little impact on the phase shifts in the physical region when using the covariant χPT formulation, while the changes are more visible in the two considered HB approaches. These observations are in line with the conclusions of section IV A. Further, as already pointed out above, using the additional

constraints from the reaction $\pi N \to \pi\pi N$ has almost no effect on the description of πN scattering in the physical region within the employed fitting procedure. As a consequence, the predictions for the phase shifts in Fig. 12 are almost identical to the ones shown in Fig. 9 of Ref. [8] for all considered counting schemes.

We now turn to the reaction $\pi N \to \pi\pi N$. As explained in section IV B, we are unable to obtain simultaneously a good description of both the $\pi N \to \pi N$ and $\pi N \to \pi\pi N$ data at order Q^4, which is mainly due to the large values of some of the $2\pi NN$ LECs d_i preferred by the elastic scattering data being seemingly incompatible with the single pion production data. Here and in what follows, we, therefore, show only a few representative examples for observables. Our results for the total cross section in five channels are shown in Fig. 13. While the description of the data at low energies used in the fit is fairly good, one observes a strong overestimation of the cross section at higher energies, which is particularly pronounced in the $\pi^+ p \to \pi^+ \pi^+ n$ and $\pi^- p \to \pi^0 \pi^- p$ channels. While the covariant approach shows the smallest deviations from the data, one observes no improvement (at both orders Q^3 and Q^4) as compared with the tree-level calculations of Ref. [35]. In Figs. 14-17, we also show selected observables in the channel $\pi^- p \to \pi^+ \pi^+ n$ which may be viewed as representative examples. Specifically, the angular correlation function W is shown as a function of the final dipion mass squared $M_{\pi\pi}^2$ for fixed angles θ_1 and θ_2 (θ_1 and ϕ_2) in Figs. 14 and 15 (Figs. 16 and 17) in comparison with the data from Ref. [60]. Further, our predictions for the single-differential cross sections with respect to $M_{\pi\pi}^2$ and t are plotted in Figs. 18 and 19 in comparison with the data from Ref. [43]. We refer the reader to Ref. [35] for details on the kinematics and for the definitions of various observables in this reaction. Comparing our predictions with the tree-level calculations reported in Ref. [35], we observe a clear improvement for the angular correlation at $\theta_1 = 76°$ and $\theta_2 = 66.7°$, $\theta_2 = 39.7°$ as well as at $\theta_1 = 71°$ and $\theta_2 = 69.4°$, $\theta_2 = 41.5°$, see the lower two panels of Figs. 14 and 15. In all remaining cases shown in Figs. 14-19, the description of the data appears to be comparable to the one reported in Ref. [35].

As already mentioned in section IV, the most probable reason for a slower convergence of the chiral expansion at higher energies are the missing contributions of the Δ and Roper resonances. A full-fledged inclusion of the Δ and Roper resonances would require calculating a number of tree-level and loop diagrams and adjusting many additional parameters, which goes beyond the scope of this work. Instead, we perform here a simplified partial inclusion of the Δ resonance by taking into account the leading Δ-pole diagrams in the πN elastic channel (as was done in Ref. [8]) and in the $\pi N \to \pi\pi N$. To avoid the introduction of additional parameters, we set the constants h_A and g_1 to their large-N_c values, see section V. Note that although the sign of g_1 can be fixed by large-N_c constraints, we also checked that using the opposite sign, $g_1 = -2.29$, has no substantial effects on the results because the Δ-pole contribution to the $\pi N \to \pi\pi N$ amplitude appears to be rather small, consistent with the findings in Ref. [50] for the reaction $\gamma N \to \pi\pi N$. On the other hand, the inclusion of the leading Δ-pole diagrams in the $\pi N \to \pi N$ channel influences indirectly the results in the $\pi N \to \pi\pi N$ channel since the obtained LECs (in particular d_i) become smaller in line with the resonance saturation, see the discussion in section V. As a result, the description of the $\pi N \to \pi\pi N$ data improves significantly. This is illustrated with the example of the total cross sections for all five channels in Fig. 20. The χ^2 ($\bar{\chi}^2$) also show a dramatic improvement for both $\pi N \to \pi N$ and $\pi N \to \pi\pi N$ reactions, and their dependence on a maximum energy in the $\pi\pi N$ channel becomes much more flat (cf. Fig. 21). This indicates a potentially better convergence of the chiral expansion in the presence of explicit Δ degrees of freedom.

The fact that the $\bar{\chi}^2_{\pi\pi N}$ slightly increases at higher energy could signal the importance of the Roper resonance, which we do not take into account explicitly.

We have reached the values of reduced $\bar{\chi}^2$ around 2(3) for the $\bar{\chi}^2_{\pi N}/\text{dof}$ ($\bar{\chi}^2_{\pi\pi N}/\text{dof}$) at order $Q^4 + \delta^1$. To obtain the values of reduced $\bar{\chi}^2$ even closer to 1 it would likely be necessary to refine the existing data base by rejecting inconsistent data sets as it is commonly done in the nucleon-nucleon sector [61, 62]. Consider a more established case of the πN data. In this case our $\bar{\chi}^2_{\pi N}$ does not differ much from the $\chi^2_{\pi N}$, which indicates that the errors are dominated by the experimental uncertainties. On the other hand, we utilize the GWU-SAID data base [23] without change, and the reduced χ^2 of the GWU-SAID partial-wave analysis [25] (for the same data base and the energy region relevant for our study) is equal to $\chi^2/\text{dof} \approx 1.8$. Clearly, we will not be able to obtain χ^2/dof smaller than this value without modifying the data base by means of rejecting some inconsistent data. This goes, however, beyond the scope of the present work.

VII. SUMMARY AND OUTLOOK

The main results of our paper can be summarized as follows:

- We have extended our analysis of pion-nucleon scattering in chiral perturbation theory to the full one-loop order (Q^3 and Q^4) reported in Ref. [8] by imposing additional constraints from the subthreshold parameters calculated by means of the Roy-Steiner equations in Ref. [3] and from the combined fit with the $\pi N \to \pi\pi N$ reaction at low energies. We have considered all three formulations of χPT, namely the heavy-baryon schemes HB-NN, HB-πN and the covariant version. For the first time, the $\pi N \to \pi\pi N$ scattering amplitude has been calculated at the chiral order Q^4. The fits to the combined data sets were performed employing the approach for estimating the theoretical uncertainty from the truncation of the chiral expansion introduced in Ref. [27].

- For the combined fit with the Roy-Steiner subthreshold parameters the extracted low-energy constants are found to have similar statistical uncertainties as in the fit to πN scattering data alone. However, we found that taking into account the additional constraints in the subthreshold region allows to strongly suppress the amount of correlations between some of the LECs. The description of the subthreshold parameters in the combined fit is obviously improved whereas the πN data in the physical region are reproduced slightly worse. The smallest change in the $\bar{\chi}^2$ (without theoretical errors) and in the values of LECs is observed for the covariant formulation of χPT.

- For the combined fit with the $\pi N \to \pi\pi N$ reaction, the extracted low-energy constants already contributing to the elastic πN amplitude and their statistical uncertainties remain nearly unchanged. As in the case of the constraints from the subthreshold region, strong correlations among LECs are found to be reduced. Some of the new LECs that give contributions to the $\pi N \to \pi\pi N$ amplitude appear to be "unnaturally" large in magnitude. However, our analysis shows that the corresponding LECs appear in the scattering amplitudes in linear combinations, which are suppressed by large numerical factors as compared to the other LECs. As a result, we do not observe any unnatural enhancement of their contributions to the scattering observables.

14

- Using the results of the combined fit to the $\pi N \to \pi N$ and $\pi N \to \pi\pi N$ reactions, we confront the results of our calculations with the experimental data for various $\pi N \to \pi\pi N$ observables as well as for the πN phase shifts. For all three formulations of χPT, we obtain a satisfactory description of the experimental/empirical data and a reasonable convergence pattern. The agreement with the data becomes worse as the energy rises. This most probably indicates the importance of the $\pi\Delta$ channel and the Roper pole, which we do not take into account explicitly. A simplified, partial inclusion of the Δ resonance via tree-level pole diagrams leads to a significant improvement in the description of the data in both $\pi N \to \pi N$ and $\pi N \to \pi\pi N$ channels in accordance with this assumption. We anticipate that a rigorous treatment of the Δ and Roper resonances as explicit degrees of freedom within χPT, extending the tree-level study of Ref. [36], will improve convergence of the theory and agreement with the data for two considered reactions and will make it possible to extend the energy region of applicability of chiral perturbation theory, see also Ref. [41]. Work along these lines is in progress.

Acknowledgments

Appendix A: Resonance saturation of the LECs

Below, we give the explicit expressions for resonance contributions to the various LECs. The contributions of the Δ degrees of freedom to the πN LECs read:

$$c_{1,\Delta} = 0\,,$$

$$c_{2,\Delta} = \frac{4h_A^2 m_N^2}{9(m_N - m_\Delta)m_\Delta^2}\,,$$

$$c_{3,\Delta} = -\frac{4h_A^2}{9(m_N - m_\Delta)}\,,$$

$$c_{4,\Delta} = \frac{2h_A^2}{9(m_N - m_\Delta)}\,,$$

$$d_{1+2,\Delta} = -\frac{h_A^2 \left(2m_N^2 - 3m_N m_\Delta + 3m_\Delta^2\right)}{18(m_N - m_\Delta)^2 m_\Delta^2}\,,$$

$$d_{3,\Delta} = \frac{h_A^2 m_N^2}{9(m_N - m_\Delta)^2 m_\Delta^2}\,,$$

$$d_{4,\Delta} = -\frac{g_A h_A^2}{36(m_N - m_\Delta)^2} - \frac{5g_1 h_A^2 \left(m_N^2 - 2m_N m_\Delta - 4m_\Delta^2\right)}{324(m_N - m_\Delta)^2 m_\Delta^2}$$
$$- \frac{h_A b_4}{18(m_N - m_\Delta)} + \frac{h_A b_5}{18(m_N - m_\Delta)}\,,$$

$$d_{5,\Delta} = -\frac{h_A^2(2m_N + m_\Delta)}{36(m_N - m_\Delta)m_\Delta^2}\,,$$

$$d_{10,\Delta} = -\frac{g_A h_A^2}{3(m_N - m_\Delta)^2} + \frac{g_1 h_A^2 \left(m_N^2 - 2m_N m_\Delta + 4m_\Delta^2\right)}{27(m_N - m_\Delta)^2 m_\Delta^2} \tag{A1}$$
$$- \frac{2h_A b_4}{3(m_N - m_\Delta)} - \frac{5h_A b_5}{9(m_N - m_\Delta)}\,,$$

$$d_{11,\Delta} = \frac{h_A b_5}{9m_N - 9m_\Delta} - \frac{g_1 h_A^2 \left(4m_N^2 - 8m_N m_\Delta + 11m_\Delta^2\right)}{81(m_N - m_\Delta)^2 m_\Delta^2}$$
$$+ \frac{g_A h_A^2}{9(m_N - m_\Delta)^2} + \frac{2h_A b_4}{9(m_N - m_\Delta)}\,,$$

$$d_{12,\Delta} = \frac{g_A h_A^2 m_N(2m_N + m_\Delta)}{9(m_N - m_\Delta)^2 m_\Delta^2} + \frac{g_1 h_A^2 m_N^2 \left(8m_N^2 + 2m_N m_\Delta - 19m_\Delta^2\right)}{81(m_N - m_\Delta)^2 m_\Delta^4}$$
$$+ \frac{2h_A b_4 m_N(2m_N + m_\Delta)}{9(m_N - m_\Delta)m_\Delta^2} + \frac{h_A b_5 m_N(2m_N + 3m_\Delta)}{9(m_N - m_\Delta)m_\Delta^2}\,,$$

$$d_{13,\Delta} = \frac{h_A b_5 m_N(2m_N - 3m_\Delta)}{9(m_N - m_\Delta)m_\Delta^2} - \frac{g_1 h_A^2 m_N^2 \left(4m_N^2 + 6m_N m_\Delta - 17m_\Delta^2\right)}{81(m_N - m_\Delta)^2 m_\Delta^4}$$
$$- \frac{2h_A b_4 m_N}{9m_N m_\Delta - 9m_\Delta^2} - \frac{g_A h_A^2 m_N}{9(m_N - m_\Delta)^2 m_\Delta}\,,$$

$$d_{14-15,\Delta} = \frac{2h_A^2 m_N}{9(m_N - m_\Delta)^2 m_\Delta}$$

$$d_{16,\Delta} = 0\,,$$

$$e_{10,\Delta} = \frac{g_A h_A^2 (3m_N - m_\Delta)}{72 m_\Delta (-m_N + m_\Delta)^3} + \frac{5 g_1 h_A^2 m_N \left(2m_N^2 - 9 m_N m_\Delta + 17 m_\Delta^2\right)}{648 (m_N - m_\Delta)^3 m_\Delta^3}$$
$$- \frac{h_A b_5 (m_N - 3m_\Delta)}{72 (m_N - m_\Delta)^2 m_\Delta} + \frac{h_A b_4 (-2m_N + m_\Delta)}{36 (m_N - m_\Delta)^2 m_\Delta},$$

$$e_{11,\Delta} = \frac{g_A h_A^2 \left(m_N^2 + m_N m_\Delta - 6 m_\Delta^2\right)}{72 m_N (m_N - m_\Delta)^2 m_\Delta (m_N + m_\Delta)}$$
$$- \frac{5 g_1 h_A^2 \left(4m_N^5 + 4m_N^4 m_\Delta + 7 m_N^3 m_\Delta^2 - 5 m_N^2 m_\Delta^3 + 18 m_N m_\Delta^4 - 12 m_\Delta^5\right)}{648 m_N (m_N - m_\Delta)^2 m_\Delta^4 (m_N + m_\Delta)}$$
$$+ \frac{b_4 \left(h_A m_N^2 + h_A m_N m_\Delta - 3 h_A m_\Delta^2\right)}{36 m_N^3 m_\Delta - 36 m_N m_\Delta^3} - \frac{b_5 \left(h_A m_N^2 + h_A m_N m_\Delta - 3 h_A m_\Delta^2\right)}{36 m_N^3 m_\Delta - 36 m_N m_\Delta^3},$$

$$e_{12,\Delta} = \frac{g_A h_A^2 \left(2m_N^3 - 7 m_N^2 m_\Delta + 13 m_N m_\Delta^2 - 6 m_\Delta^3\right)}{72 m_N (m_N - m_\Delta)^3 m_\Delta^2}$$
$$+ \frac{5 g_1 h_A^2 \left(4m_N^5 + 4m_N^4 m_\Delta - 33 m_N^3 m_\Delta^2 + 45 m_N^2 m_\Delta^3 - 42 m_N m_\Delta^4 + 12 m_\Delta^5\right)}{648 m_N (m_N - m_\Delta)^3 m_\Delta^4}$$
$$+ \frac{h_A b_4 \left(2m_N^3 - 5 m_N^2 m_\Delta + 7 m_N m_\Delta^2 - 3 m_\Delta^3\right)}{36 m_N (m_N - m_\Delta)^2 m_\Delta^2}$$
$$- \frac{h_A b_5 \left(2m_N^3 - 5 m_N^2 m_\Delta + 7 m_N m_\Delta^2 - 3 m_\Delta^3\right)}{36 m_N (m_N - m_\Delta)^2 m_\Delta^2},$$

$$e_{13,\Delta} = \frac{g_A h_A^2 m_N \left(-3m_N^2 + m_\Delta^2\right)}{36 (m_N - m_\Delta)^3 m_\Delta^2 (m_N + m_\Delta)} + \frac{5 g_1 h_A^2 m_N^2 \left(4m_N^2 - 6 m_N m_\Delta - 3 m_\Delta^2\right)}{162 m_\Delta^3 (-m_N + m_\Delta)^3 (m_N + m_\Delta)}$$
$$- \frac{h_A b_4 m_N^3}{18 (m_N - m_\Delta)^2 m_\Delta^2 (m_N + m_\Delta)} + \frac{h_A b_5 m_N^3}{18 (m_N - m_\Delta)^2 m_\Delta^2 (m_N + m_\Delta)},$$

$$e_{14,\Delta} = \frac{h_A^2 \left(2m_N^2 - m_N m_\Delta + 3 m_\Delta^2\right)}{72 (m_N - m_\Delta)^2 m_\Delta^2 (m_N + m_\Delta)},$$

$$e_{15,\Delta} = \frac{h_A^2 m_N \left(m_N^2 - m_N m_\Delta + m_\Delta^2\right)}{9 m_\Delta^2 (-m_N + m_\Delta)^3 (m_N + m_\Delta)},$$

$$e_{16,\Delta} = \frac{h_A^2 m_N^3}{9 (m_N - m_\Delta)^3 m_\Delta^2 (m_N + m_\Delta)},$$

$$e_{17,\Delta} = -\frac{h_A^2 \left(m_N^2 - 2m_N m_\Delta + 3 m_\Delta^2\right)}{72 m_N (m_N - m_\Delta)^2 m_\Delta (m_N + m_\Delta)},$$

$$e_{18,\Delta} = \frac{h_A^2 m_N \left(m_N^2 - 4m_N m_\Delta + m_\Delta^2\right)}{36 m_\Delta^2 (-m_N + m_\Delta)^3 (m_N + m_\Delta)},$$

$$e_{34,\Delta} = -\frac{g_A h_A^2 \left(2m_N^2 + 6 m_N m_\Delta + 5 m_\Delta^2\right)}{72 m_N (m_N - m_\Delta) m_\Delta^2 (m_N + m_\Delta)}$$
$$- \frac{5 g_1 h_A^2 \left(4m_N^5 + 8 m_N^4 m_\Delta - 11 m_N^3 m_\Delta^2 - 19 m_N^2 m_\Delta^3 - 6 m_N m_\Delta^4 + 12 m_\Delta^5\right)}{648 m_N (m_N - m_\Delta)^2 m_\Delta^4 (m_N + m_\Delta)}$$
$$+ \frac{h_A b_4 \left(-2m_N^3 - 3 m_N^2 m_\Delta + m_N m_\Delta^2 + 3 m_\Delta^3\right)}{36 m_\Delta^2 \left(m_N^3 - m_N m_\Delta^2\right)}$$
$$+ \frac{h_A b_5 \left(2m_N^3 + 3 m_N^2 m_\Delta - m_N m_\Delta^2 - 3 m_\Delta^3\right)}{36 m_\Delta^2 \left(m_N^3 - m_N m_\Delta^2\right)},$$

$$\text{(A2)}$$

and

$$2e_{19,\Delta} - e_{22,\Delta} - \hat{e}_{36,\Delta} = 0\,,$$

$$e_{20,\Delta} + e_{35,\Delta} = -\frac{h_A^2 m_N(m_N + 2m_\Delta)}{18(m_N - m_\Delta)^2 m_\Delta^2(m_N + m_\Delta)}\,,$$

$$2e_{21,\Delta} - e_{37,\Delta} = -\frac{h_A^2}{36m_N^2 m_\Delta - 36m_N m_\Delta^2}\,,$$ (A3)

$$e_{22,\Delta} - 4e_{38,\Delta} = \frac{h_A^2(2m_N + 3m_\Delta)}{36m_\Delta^2\left(m_N^2 - m_\Delta^2\right)}\,.$$

Whereas the contributions of the explicit Roper resonance have the form

$$c_{1,R} = 0\,,$$

$$c_{2,R} = \frac{g_{RN}^2 m_N}{2m_N^2 - 2m_R^2}\,,$$

$$c_{3,R} = -\frac{g_{RN}^2}{4(m_N - m_R)}\,,$$

$$c_{4,R} = \frac{g_{RN}^2}{2m_N - 2m_R}\,,$$

$$d_{1+2,R} = \frac{g_{RN}^2(3m_N - m_R)}{8(m_N - m_R)^2(m_N + m_R)}\,,$$

$$d_{3,R} = -\frac{g_{RN}^2 m_N^2}{2(m_N - m_R)^2(m_N + m_R)^2}\,,$$

$$d_{4,R} = -\frac{g_A g_{RN}^2}{16(m_N - m_R)^2} + \frac{g_{R\Delta}g_{RN}h_A}{18(m_N - m_R)(m_N - m_\Delta)}$$
$$+ \frac{g_{RN}^2 g_{RR}}{16(m_N - m_R)^2} - \frac{g_{RN}c_4^R}{4(m_N - m_R)}\,,$$

$$d_{5,R} = 0\,,$$ (A4)

$$d_{10,R} = -\frac{3g_A g_{RN}^2}{8(m_N - m_R)^2} + \frac{2g_{R\Delta}g_{RN}h_A}{3(m_N - m_R)(m_N - m_\Delta)}$$
$$+ \frac{3g_{RN}^2 g_{RR}}{8(m_N - m_R)^2} + \frac{g_{RN}c_3^R}{m_N - m_R} - \frac{g_{RN}c_4^R}{m_N - m_R}\,,$$

$$d_{11,R} = \frac{g_A g_{RN}^2}{4(m_N - m_R)^2} - \frac{2g_{R\Delta}g_{RN}h_A}{9(m_N - m_R)(m_N - m_\Delta)}$$
$$- \frac{g_{RN}^2 g_{RR}}{4(m_N - m_R)^2} + \frac{g_{RN}c_4^R}{m_N - m_R}\,,$$

$$d_{12,R} = \frac{g_A g_{RN}^2\left(5m_N^2 + 2m_N m_R - m_R^2\right)}{4\left(m_N^2 - m_R^2\right)^2}$$
$$- \frac{2g_{R\Delta}g_{RN}h_A m_N\left(2m_N^2 + m_N(2m_R - m_\Delta) + m_\Delta(m_R + 2m_\Delta)\right)}{9\left(m_N^2 - m_R^2\right)(m_N - m_\Delta)m_\Delta^2}$$
$$- \frac{g_{RN}^2 g_{RR}m_N(m_N + 2m_R)}{2\left(m_N^2 - m_R^2\right)^2} + \frac{g_{RN}c_2^R}{m_N - m_R} + \frac{2g_{RN}c_4^R m_N}{m_N^2 - m_R^2}\,,$$

$$d_{13,R} = -\frac{g_A g_{RN}^2 (3m_N - m_R)}{4(m_N - m_R)^2(m_N + m_R)} - \frac{2g_{R\Delta} g_{RN} h_A m_N (m_N - m_R - 2m_\Delta)}{9\left(m_N^2 - m_R^2\right)(m_N - m_\Delta)m_\Delta}$$

$$+ \frac{g_{RN}^2 g_{RR} m_N m_R}{\left(m_N^2 - m_R^2\right)^2} - \frac{2g_{RN} c_4^R m_N}{m_N^2 - m_R^2},$$

$$d_{14-15,R} = -\frac{g_{RN}^2}{4(m_N - m_R)^2},$$

$$d_{16,R} = \frac{2g_{RN} c_1^R}{m_N - m_R},$$

$$e_{10,R} = -\frac{g_{RN}^2 g_{RR}}{8(m_N - m_R)^3}$$

$$+ \frac{g_{R\Delta} g_{RN} h_A \left(2m_N^2 + m_\Delta(m_R + 2m_\Delta) - m_N(2m_R + 3m_\Delta)\right)}{36(m_N - m_R)^2(m_N - m_\Delta)^2 m_\Delta}$$

$$+ \frac{g_A g_{RN}^2 (5m_N - m_R)}{32 m_N (m_N - m_R)^3} + \frac{g_{RN} c_4^R}{4(m_N - m_R)^2},$$

$$e_{11,R} = -\frac{g_A g_{RN}^2 m_R}{8m_N(m_N - m_R)^2(m_N + m_R)}$$

$$+ \frac{g_{R\Delta} g_{RN} h_A \left(m_N^3 - m_N^2(m_R - 5m_\Delta) + 3m_R m_\Delta^2 + m_N m_\Delta(-m_R + m_\Delta)\right)}{36 m_N \left(m_N^2 - m_R^2\right) m_\Delta \left(m_N^2 - m_\Delta^2\right)}$$

$$+ \frac{g_{RN}^2 g_{RR} \left(3m_N^2 + 2m_N m_R + 3m_R^2\right)}{32 m_N \left(m_N^2 - m_R^2\right)^2} - \frac{g_{RN} c_4^R (m_N + 3m_R)}{8\left(m_N^3 - m_N m_R^2\right)},$$

$$e_{12,R} = -\frac{g_{RN} c_4^R \left(3m_N^2 - 2m_N m_R + 3m_R^2\right)}{8m_N(m_N - m_R)^2(m_N + m_R)}$$

$$- \frac{g_{R\Delta} g_{RN} h_A}{36 m_N(m_N - m_R)^2(m_N + m_R)(m_N - m_\Delta)^2 m_\Delta^2}\Big(2m_N^5 - m_N^4 m_\Delta$$

$$+ 3m_R^2 m_\Delta^3 - m_N m_R m_\Delta^2(7m_R + 2m_\Delta) - m_N^3 \left(2m_R^2 + 4m_R m_\Delta + 3m_\Delta^2\right)$$

$$+ m_N^2 m_\Delta \left(5m_R^2 + 6m_R m_\Delta + 3m_\Delta^2\right)\Big)$$

$$- \frac{g_A g_{RN}^2 \left(3m_N^3 + m_R^3\right)}{8m_N(m_N - m_R)^3(m_N + m_R)^2} + \frac{g_{RN}^2 g_{RR} \left(5m_N^3 + 9m_N^2 m_R - m_N m_R^2 + 3m_R^3\right)}{32 m_N(m_N - m_R)^3(m_N + m_R)^2},$$

$$e_{13,R} = \frac{g_A g_{RN}^2 m_N \left(7m_N^2 + 2m_N m_R - m_R^2\right)}{8\left(m_N^2 - m_R^2\right)^3}$$

$$+ \frac{g_{R\Delta} g_{RN} h_A m_N^2}{18\left(m_N^2 - m_R^2\right)^2 (m_N - m_\Delta)^2 m_\Delta^2 (m_N + m_\Delta)}\Big(m_N^4 + m_N^3(m_R + 3m_\Delta)$$

$$+ m_\Delta^2 \left(m_R^2 + 2m_R m_\Delta + 4m_\Delta^2\right)$$

$$- m_N^2 \left(m_R^2 + 2m_R m_\Delta + 5m_\Delta^2\right) - m_N \left(m_R^3 + m_R^2 m_\Delta + 2m_\Delta^3\right)\Big)$$

$$- \frac{g_{RN}^2 g_{RR} m_N^2(m_N + 3m_R)}{4\left(m_N^2 - m_R^2\right)^3} + \frac{g_{RN} c_4^R m_N^2}{\left(m_N^2 - m_R^2\right)^2},$$

$$\text{(A5)}$$

19

$$e_{14,R} = \frac{g_{RN}^2(3m_N - m_R)}{64m_N(m_N - m_R)^2(m_N + m_R)} \, ,$$

$$e_{15,R} = -\frac{g_{RN}^2 m_N(2m_N - m_R)}{8(m_N - m_R)^3(m_N + m_R)^2} \, ,$$

$$e_{16,R} = \frac{g_{RN}^2 m_N^3}{4(m_N - m_R)^3(m_N + m_R)^3} \, ,$$

$$e_{17,R} = -\frac{g_{RN}^2}{32m_N(m_N - m_R)^2} \, ,$$

$$e_{18,R} = \frac{g_{RN}^2 m_N}{8(m_N - m_R)^3(m_N + m_R)} \, , \tag{A6}$$

$$e_{34,R} = \frac{3g_A g_{RN}^2}{32m_N(m_N - m_R)^2}$$

$$+ \frac{g_{R\Delta} g_{RN} h_A}{36m_N(m_N - m_R)(m_N + m_R)m_\Delta^2 (m_N^2 - m_\Delta^2)}\Big(2m_N^4 + 3m_N^2(m_R - m_\Delta)m_\Delta$$

$$- 3m_R m_\Delta^3 - m_N m_\Delta^2(m_R + 3m_\Delta) + m_N^3(2m_R + 3m_\Delta)\Big)$$

$$- \frac{3g_{RN}^2 g_{RR}}{32m_N(m_N - m_R)^2} + \frac{3g_{RN}c_4^R}{8m_N^2 - 8m_N m_R} \, ,$$

and

$$e_{20,R} + \hat{e}_{35,R} = 0 \, ,$$

$$2e_{21,R} - e_{37,R} = 0 \, ,$$

$$2e_{19,R} - e_{22,R} - e_{36,R} = -\frac{g_{RN}^2}{16\left(m_N^3 - m_N m_R^2\right)} \, , \tag{A7}$$

$$e_{22,R} - e_{34,R} = \frac{g_{RN}^2}{32m_N^3 - 32m_N m_R^2} \, .$$

[1] C. Ditsche, M. Hoferichter, B. Kubis and Ulf-G. Meißner, JHEP **1206**, 043 (2012) [arXiv:1203.4758 [hep-ph]].

[2] M. Hoferichter, J. Ruiz de Elvira, B. Kubis and Ulf-G. Meißner, Phys. Rev. Lett. **115**, 092301 (2015) [arXiv:1506.04142 [hep-ph]].

[3] M. Hoferichter, J. Ruiz de Elvira, B. Kubis and Ulf-G. Meißner, Phys. Rept. **625**, 1 (2016) [arXiv:1510.06039 [hep-ph]].

[4] E. E. Jenkins and A. V. Manohar, Phys. Lett. B **255**, 558 (1991).

[5] V. Bernard, N. Kaiser, J. Kambor and Ulf-G. Meißner, Nucl. Phys. B **388**, 315 (1992).

[6] S. Weinberg, Nucl. Phys. B **363**, 3 (1991).

[7] E. Epelbaum, H. W. Hammer and Ulf-G. Meißner, Rev. Mod. Phys. **81**, 1773 (2009) [arXiv:0811.1338 [nucl-th]].

[8] D. Siemens, V. Bernard, E. Epelbaum, A. Gasparyan, H. Krebs and Ulf-G. Meißner, Phys. Rev. C **94**, 014620 (2016) [arXiv:1602.02640 [nucl-th]].

[9] P. J. Ellis and H. B. Tang, Phys. Rev. C **57**, 3356 (1998) [hep-ph/9709354].

[10] T. Becher and H. Leutwyler, Eur. Phys. J. C **9**, 643 (1999) [hep-ph/9901384].

[11] J. Gegelia and G. Japaridze, Phys. Rev. D **60**, 114038 (1999) [hep-ph/9908377].

[12] T. Fuchs, J. Gegelia, G. Japaridze and S. Scherer, Phys. Rev. D **68**, 056005 (2003) [hep-ph/0302117].

[13] M. Mojzis, Eur. Phys. J. C **2**, 181 (1998) [hep-ph/9704415].

[14] N. Fettes, Ulf-G. Meißner and S. Steininger, Nucl. Phys. A **640**, 199 (1998) [hep-ph/9803266].

[15] P. Buettiker and Ulf-G. Meißner, Nucl. Phys. A **668**, 97 (2000) [hep-ph/9908247].

[16] N. Fettes, Ulf-G. Meißner, M. Mojzis and S. Steininger, Annals Phys. **283**, 273 (2000) [Annals Phys. **288**, 249 (2001)] [hep-ph/0001308].

[17] N. Fettes and Ulf-G. Meißner, Nucl. Phys. A **676**, 311 (2000) [hep-ph/0002162].

[18] T. Becher and H. Leutwyler, JHEP **0106**, 017 (2001) [hep-ph/0103263].

[19] M. Hoferichter, B. Kubis and Ulf-G. Meißner, Nucl. Phys. A **833**, 18 (2010) [arXiv:0909.4390 [hep-ph]].

[20] A. Gasparyan and M. F. M. Lutz, Nucl. Phys. A **848**, 126 (2010) [arXiv:1003.3426 [hep-ph]].

[21] J. M. Alarcon, J. Martin Camalich and J. A. Oller, Annals Phys. **336**, 413 (2013) [arXiv:1210.4450 [hep-ph]].

[22] Y. H. Chen, D. L. Yao and H. Q. Zheng, Phys. Rev. D **87**, 054019 (2013) [arXiv:1212.1893 [hep-ph]].

[23] R. L. Workman, R. A. Arndt, W. J. Briscoe, M. W. Paris and I. I. Strakovsky, Phys. Rev. C **86**, 035202 (2012) [arXiv:1204.2277 [hep-ph]].

[24] R. Koch, Nucl. Phys. A **448**, 707 (1986).

[25] R. A. Arndt, W. J. Briscoe, I. I. Strakovsky and R. L. Workman, Phys. Rev. C **74**, 045205 (2006) [nucl-th/0605082].

[26] K. A. Wendt, B. D. Carlsson and A. Ekström, arXiv:1410.0646 [nucl-th].

[27] E. Epelbaum, H. Krebs and Ulf-G. Meißner, Eur. Phys. J. A **51**, no. 5, 53 (2015) [arXiv:1412.0142 [nucl-th]].

[28] D. L. Yao, D. Siemens, V. Bernard, E. Epelbaum, A. M. Gasparyan, J. Gegelia, H. Krebs and Ulf-G. Meißner, JHEP **1605**, 038 (2016) [arXiv:1603.03638 [hep-ph]].

[29] V. Bernard, N. Kaiser and Ulf-G. Meißner, Nucl. Phys. B **457**, 147 (1995) [hep-ph/9507418].

[30] N. Fettes, V. Bernard and Ulf-G. Meißner, Nucl. Phys. A **669**, 269 (2000) [hep-ph/9907276].

[31] J. Beringer, PiN Newslett. **7**, 33 (1992).

[32] V. Bernard, N. Kaiser and Ulf-G. Meißner, Phys. Lett. B **332**, 415 (1994) Erratum: [Phys. Lett. B **338**, 520 (1994)] [hep-ph/9404236].

[33] M. G. Olsson, Ulf-G. Meißner, N. Kaiser and V. Bernard, PiN Newslett. **10**, 201 (1995) [hep-ph/9503237].

[34] V. Bernard, N. Kaiser and Ulf-G. Meißner, Nucl. Phys. A **619**, 261 (1997) [hep-ph/9703218].

[35] D. Siemens, V. Bernard, E. Epelbaum, H. Krebs and Ulf-G. Meißner, Phys. Rev. C **89**, no. 6, 065211 (2014)

[36] T. S. Jensen and A. F. Miranda, Phys. Rev. C **55**, 1039 (1997).

[37] G. Höhler, in Landolt-Börnstein, **9b2**, ed. H. Schopper (Springer, Berlin, 1983).

[38] M. Hoferichter, J. Ruiz de Elvira, B. Kubis and Ulf-G. Meißner, Phys. Rev. Lett. **115**, no. 19, 192301 (2015) [arXiv:1507.07552 [nucl-th]].

[39] R. J. Furnstahl, D. R. Phillips and S. Wesolowski, J. Phys. G **42**, no. 3, 034028 (2015) [arXiv:1407.0657 [nucl-th]].

[40] S. Wesolowski, N. Klco, R. J. Furnstahl, D. R. Phillips and A. Thapaliya, J. Phys. G **43**, no. 7, 074001 (2016) [arXiv:1511.03618 [nucl-th]].

[41] D. Siemens, J. Ruiz de Elvira, E. Epelbaum, M. Hoferichter, H. Krebs, B. Kubis and Ulf-G. Meißner, Phys. Lett. B **770**, 27 (2017) [arXiv:1610.08978 [nucl-th]].

[42] V. V. Vereshagin, S. G. Sherman, A. N. Manashov, U. Bohnert, M. Dillig, W. Eyrich, O. Jakel and M. Moosburger, Nucl. Phys. A **592**, 413 (1995)

[43] M. Kermani *et al.* [CHAOS Collaboration], Phys. Rev. C **58**, 3419 (1998).

[44] J. B. Lange, F. Duncan, A. Ambardar, A. Feltham, G. Hofman, R. R. Johnson, G. Jones and M. Pavan *et al.*, Phys. Rev. Lett. **80**, 1597 (1998).

[45] S. Prakhov *et al.* [Crystal Ball Collaboration], Phys. Rev. C **69**, 045202 (2004).

[46] D. M. Manley, Phys. Rev. D **30**, 536 (1984).

[47] J. Bijnens and G. Ecker, Ann. Rev. Nucl. Part. Sci. **64**, 149 (2014) [arXiv:1405.6488 [hep-ph]].

[48] S. Aoki *et al.*, Eur. Phys. J. C **77** (2017) no.2, 112 [arXiv:1607.00299 [hep-lat]].

[49] C. Patrignani *et al.* [Particle Data Group], Chin. Phys. C **40**, no. 10, 100001 (2016).

[50] V. Bernard, N. Kaiser, Ulf-G. Meißner and A. Schmidt, Nucl. Phys. A **580**, 475 (1994) [nucl-th/9403013].

[51] V. Pascalutsa and D. R. Phillips, Phys. Rev. C **67**, 055202 (2003) [nucl-th/0212024].

[52] B. Long and U. van Kolck, Nucl. Phys. A **870-871**, 72 (2011) [arXiv:1105.2764 [nucl-th]].

[53] R. J. Furnstahl, N. Klco, D. R. Phillips and S. Wesolowski, Phys. Rev. C **92**, no. 2, 024005 (2015) [arXiv:1506.01343 [nucl-th]].

[54] J. A. Melendez, S. Wesolowski and R. J. Furnstahl, Phys. Rev. C **96**, no. 2, 024003 (2017) [arXiv:1704.03308 [nucl-th]].

[55] V. Bernard, N. Kaiser and Ulf-G. Meißner, Nucl. Phys. A **615**, 483 (1997) [hep-ph/9611253].

[56] H. Krebs, E. Epelbaum and Ulf-G. Meißner, Eur. Phys. J. A **32**, 127 (2007) [nucl-th/0703087].

[57] B. Borasoy, P. C. Bruns, Ulf-G. Meißner and R. Lewis, Phys. Lett. B **641**, 294 (2006) [hep-lat/0608001].

[58] T. R. Hemmert, UMI-98-09346.

[59] T. R. Hemmert, B. R. Holstein and J. Kambor, J. Phys. G **24**, 1831 (1998) [hep-ph/9712496].

[60] R. Müller, R. Baran, U. Bohnert, P. Helbig, G. Herrmann, A. Hofmann, O. Jaekel and H. Kruger *et al.*, Phys. Rev. C **48**, 981 (1993).

[61] V. G. J. Stoks, R. A. M. Klomp, M. C. M. Rentmeester and J. J. de Swart, Phys. Rev. C **48**, 792 (1993).

[62] R. Navarro Prez, J. E. Amaro and E. Ruiz Arriola, Phys. Rev. C **88**, no. 6, 064002 (2013) Erratum: [Phys. Rev. C **91**, no. 2, 029901 (2015)] [arXiv:1310.2536 [nucl-th]].

	HB-NN		HB-πN		Cov	
Q^2	πN	πN+RS	πN	πN+RS	πN	πN+RS
c_1	-1.82(5)	-1.69(4)	-1.92(5)	-1.60(5)	-2.16(5)	-2.12(5)
c_2	2.97(9)	3.17(8)	3.12(9)	3.63(9)	2.55(7)	2.65(7)
c_3	-6.08(6)	-6.07(5)	-6.23(6)	-6.24(5)	-6.23(5)	-6.28(5)
c_4	4.19(5)	4.61(2)	4.65(4)	5.22(3)	4.32(2)	4.32(2)
$\chi^2_{\pi N}/$dof	0.72	0.69	0.69	0.60	0.67	0.69
$\bar{\chi}^2_{\pi N}/$dof	116	128	98	121	413	402
Q^3	πN	πN+RS	πN	πN+RS	πN	πN+RS
c_1	-1.66(3)	-1.24(2)	-1.62(2)	-1.64(2)	-1.66(2)	-1.55(2)
c_2	4.10(5)	4.89(5)	3.42(4)	3.51(3)	3.42(3)	3.60(4)
c_3	-7.11(2)	-7.25(2)	-6.52(2)	-6.63(2)	-6.51(2)	-6.54(2)
c_4	4.14(5)	4.74(4)	3.89(4)	4.01(4)	3.78(4)	3.86(3)
d_{1+2}	2.78(5)	3.39(4)	3.89(5)	4.37(4)	4.07(4)	4.09(4)
d_3	-1.90(8)	-3.47(7)	-2.53(9)	-3.34(7)	-2.43(4)	-2.50(4)
d_5	-0.64(5)	0.00(4)	-0.79(5)	-0.56(4)	-0.89(4)	-0.86(4)
d_{14-15}	-7.41(12)	-7.39(13)	-6.94(14)	-7.49(13)	-6.18(10)	-6.05(10)
$\chi^2_{\pi N}/$dof	1.04	1.04	1.03	0.83	0.97	1.05
$\bar{\chi}^2_{\pi N}/$dof	14.6	14.1	13.0	14.4	13.5	13.0
Q^4	πN	πN+RS	πN	πN+RS	πN	πN+RS
c_1	-0.44(4)	-1.31(8)	0.12(5)	-1.15(8)	-0.81(4)	-0.82(7)
c_2	4.32(9)	1.88(23)	4.99(13)	2.39(22)	3.87(8)	3.56(16)
c_3	-4.40(7)	-4.43(9)	-3.09(9)	-4.44(9)	-4.91(9)	-4.59(9)
c_4	4.07(11)	3.24(17)	3.60(12)	3.45(17)	4.06(10)	3.44(13)
d_{1+2}	6.51(6)	5.95(9)	5.54(6)	5.60(9)	5.63(4)	5.43(5)
d_3	-6.21(6)	-5.64(6)	-4.40(4)	-3.84(4)	-4.75(6)	-4.58(8)
d_5	-0.07(3)	-0.11(4)	-0.45(4)	-0.89(4)	-0.42(3)	-0.40(4)
d_{14-15}	-12.08(8)	-11.61(9)	-9.42(6)	-9.45(8)	-10.18(6)	-9.94(7)
e_{14}	-0.39(24)	0.86(29)	-3.23(30)	1.28(32)	-0.85(22)	-0.63(24)
e_{15}	-6.94(51)	-11.36(81)	-7.98(53)	-13.26(79)	-5.60(39)	-7.33(45)
e_{16}	1.62(30)	10.73(95)	-0.19(24)	8.29(95)	0.39(17)	1.86(37)
e_{17}	0.73(40)	-0.66(46)	3.53(41)	-0.73(47)	-1.15(30)	-0.90(32)
e_{18}	-0.17(52)	4.47(87)	-0.05(56)	4.17(90)	1.60(35)	3.17(45)
$\chi^2_{\pi N}/$dof	1.90	1.92	1.83	2.04	1.94	2.07
$\bar{\chi}^2_{\pi N}/$dof	4.5	4.8	4.1	5.9	4.9	5.1

TABLE I: LECs determined from fits including χ^2_{RS} as additional constraints at orders Q^2, Q^3, Q^4 in comparison with the values given in [8]. The values of the πN LECs at orders Q^2, Q^3, Q^4 are given in units of GeV^{-1}, GeV^{-2} and GeV^{-3}, respectively.

	HB-NN		HB-πN		Cov	
Q^2	πN	$\pi N+\pi\pi N$	πN	$\pi N+\pi\pi N$	πN	$\pi N+\pi\pi N$
c_1	-1.69(4)	-1.69(4)	-1.60(5)	-1.59(5)	-2.19(5)	-2.12(5)
c_2	3.18(8)	3.17(8)	3.63(9)	3.65(9)	2.52(7)	2.65(7)
c_3	-6.08(5)	-6.07(5)	-6.24(5)	-6.25(6)	-6.25(6)	-6.28(5)
c_4	4.61(2)	4.61(2)	5.22(3)	5.27(4)	4.32(2)	4.32(2)
$\chi^2_{\pi N}/\mathrm{dof}$	0.72	0.72	0.69	0.69	0.67	0.67
$\bar{\chi}^2_{\pi N}/\mathrm{dof}$	116	116	98	97	413	415
$\chi^2_{\pi\pi N}/\mathrm{dof}$	-	1.03	-	0.95	-	1.09
$\bar{\chi}^2_{\pi\pi N}/\mathrm{dof}$	-	34	-	27	-	5.5
Q^3	πN	$\pi N+\pi\pi N$	πN	$\pi N+\pi\pi N$	πN	$\pi N+\pi\pi N$
c_1	-1.24(2)	-1.24(2)	-1.64(2)	-1.64(2)	-1.55(2)	-1.55(2)
c_2	4.89(5)	4.89(5)	3.51(3)	3.51(3)	3.60(4)	3.60(4)
c_3	-7.25(2)	-7.26(2)	-6.63(2)	-6.63(2)	-6.54(2)	-6.54(2)
c_4	4.74(4)	4.74(4)	4.01(4)	4.01(4)	3.86(3)	3.86(3)
d_{1+2}	3.39(4)	3.39(4)	4.37(4)	4.37(4)	4.09(4)	4.09(4)
d_3	-3.47(7)	-3.44(7)	-3.34(7)	-3.35(7)	-2.50(4)	-2.50(4)
d_4	-	3.7(2.3)	-	3.1(2.2)	-	3.3(2.1)
d_5	0.00(4)	-0.02(4)	-0.56(4)	-0.56(4)	-0.86(4)	-0.85(4)
d_{10}	-	10.9(5.6)	-	-0.8(4.9)	-	-6.4(4.6)
d_{11}	-	-30.9(7.6)	-	-15.6(6.7)	-	-1.7(6.6)
d_{12}	-	-10.9(6.0)	-	5.9(5.4)	-	11.6(4.7)
d_{13}	-	27.7(7.7)	-	13.6(6.8)	-	-1.9(6.4)
d_{14-15}	-7.39(13)	-7.36(13)	-7.49(13)	-7.43(13)	-6.05(10)	-6.02(10)
d_{16}	-	-3.0(1.6)	-	0.4(1.3)	-	0.5(1.1)
l_1	-	-0.39(60)	-	-0.39(60)	-	-0.35(60)
l_2	-	4.30(10)	-	4.29(10)	-	4.30(10)
l_3	-	3.0(2.4)	-	3.2(2.4)	-	3.2(2.4)
l_4	-	4.40(20)	-	4.41(20)	-	4.40(20)
$\chi^2_{\pi N}/\mathrm{dof}$	1.04	1.01	1.03	1.00	0.97	0.97
$\bar{\chi}^2_{\pi N}/\mathrm{dof}$	14.6	14.6	13.0	13.1	13.5	13.6
$\chi^2_{\pi\pi N}/\mathrm{dof}$	-	0.72	-	1.00	-	0.96
$\bar{\chi}^2_{\pi\pi N}/\mathrm{dof}$	-	5.3	-	6.5	-	8.0

TABLE II: LECs determined from fits at orders Q^2 and Q^3 with additional constraints from the reaction $\pi N \to \pi\pi N$ with $T_{\pi,\pi\pi N} < 275$ MeV. The values of the πN LECs at orders Q^2 and Q^3 are given in units of GeV^{-1} and GeV^{-2}, respectively, while the l_i's are dimensionless.

Q^4	HB-NN		HB-πN		Cov	
	πN	πN+$\pi\pi$N	πN	πN+$\pi\pi$N	πN	πN+$\pi\pi$N
c_1	-1.31(8)	-1.06(6)	-1.15(8)	-1.03(6)	-0.82(7)	-0.89(6)
c_2	1.88(23)	2.44(17)	2.39(22)	2.52(18)	3.56(16)	3.38(15)
c_3	-4.43(9)	-4.29(9)	-4.44(9)	-4.24(9)	-4.59(9)	-4.59(9)
c_4	3.24(17)	3.10(15)	3.45(17)	3.03(15)	3.44(13)	3.31(13)
d_{1+2}	5.95(9)	5.85(8)	5.60(9)	5.35(8)	5.43(5)	5.40(5)
d_3	-5.64(6)	-5.58(6)	-3.84(4)	-3.76(4)	-4.58(8)	-4.60(7)
d_4	-	-1.8(1.5)	-	-1.5(1.2)	-	-4.3(1.5)
d_5	-0.11(4)	-0.08(4)	-0.89(4)	-0.80(4)	-0.40(4)	-0.37(4)
d_{10}	-	-24.7(3.7)	-	-29.6(2.2)	-	-31.9(2.6)
d_{11}	-	2.9(5.0)	-	13.1(3.0)	-	20.5(3.9)
d_{12}	-	25.2(3.9)	-	28.1(2.2)	-	34.0(2.7)
d_{13}	-	-7.1(5.1)	-	-16.3(3.0)	-	-24.2(3.7)
d_{14-15}	-11.61(9)	-11.51(9)	-9.45(8)	-9.24(7)	-9.94(7)	-9.88(7)
d_{16}	-	4.11(96)	-	9.16(85)	-	0.82(80)
e_{10}	-	-34.4(8.1)	-	-33.8(7.9)	-	-22.8(6.3)
e_{11}	-	4.4(4.5)	-	13.9(5.2)	-	3.6(5.4)
e_{12}	-	56.1(4.3)	-	53.2(3.9)	-	23.5(3.9)
e_{13}	-	-57.5(7.1)	-	-61.9(7.7)	-	-19.8(6.4)
e_{14}	0.86(29)	0.81(29)	1.28(32)	1.35(31)	-0.63(24)	-0.58(24)
e_{15}	-11.36(81)	-11.39(78)	-13.26(79)	-14.11(77)	-7.33(45)	-7.48(45)
e_{16}	10.73(95)	9.15(78)	8.29(95)	8.38(81)	1.86(37)	2.22(36)
e_{17}	-0.66(46)	-0.80(46)	-0.73(47)	-1.01(47)	-0.90(32)	-0.83(32)
e_{18}	4.47(87)	5.20(81)	4.17(90)	6.14(82)	3.17(45)	3.49(44)
e_{34}	-	-0.9(15.5)	-	-11.8(18.0)	-	3.8(21.6)
l_1	-	-0.36(60)	-	-0.40(60)	-	-0.29(60)
l_2	-	4.29(10)	-	4.29(10)	-	4.29(10)
l_3	-	3.1(2.4)	-	2.9(2.4)	-	3.3(2.4)
l_4	-	4.42(20)	-	4.42(20)	-	4.39(20)
$\chi^2_{\pi N}$/dof	1.90	1.90	1.83	1.83	1.94	1.90
$\bar{\chi}^2_{\pi N}$/dof	4.5	4.6	4.1	4.1	4.9	4.9
$\chi^2_{\pi\pi N}$/dof	-	2.1	-	2.8	-	2.5
$\bar{\chi}^2_{\pi\pi N}$/dof	-	12	-	17	-	6.3

TABLE III: LECs determined from fits at order Q^4 with additional constraints from the reaction $\pi N \to \pi\pi N$ with $T_{\pi,\pi\pi N} < 275$ MeV. The values of the πN LECs at orders Q^2, Q^3, Q^4 are given in units of GeV^{-1}, GeV^{-2} and GeV^{-3}, respectively, while the l_i's are dimensionless.

d_4	-5.4(1.7)	e_{10}	-9.3(8.4)
d_{10}	-33.2(5.8)	e_{11}	4.9(6.3)
d_{11}	18.2(8.5)	e_{12}	7.3(4.6)
d_{12}	30.8(6.2)	e_{13}	-11.4(6.6)
d_{13}	-20.0(8.3)	e_{34}	-6.7(20.9)
d_{16}	1.7(1.0)		

	d_{10}	d_{11}	d_{12}	d_{13}
d_{10}		-70	-97	67
d_{11}	-89		72	-99
d_{12}	-99	88		-73
d_{13}	91	-100	-90	

TABLE IV: The left table shows $3\pi NN$ LECs determined from covariant fits at order $Q^4 + \delta^1$ with $T_{\pi,\pi\pi N} < 275$ MeV. The upper/lower triangle in the right table correspond to a selected part of the correlation matrix for the covariant fits at $Q^4/Q^4 + \delta^1$. The values of the LECs d_i and e_i are given in units of GeV^{-2} and GeV^{-3}, respectively.

Q^4	Cov	Δx	$\overline{\Delta x}$	$x_\Delta(h_A \pm g_1 \pm b_4 \pm b_5)$	$x_R(g_{RN} \pm g_{R\Delta} \pm g_{RR} \pm c^R_{1,2,3,4})$
c_1	-0.89(6)	0.03	-32	0.01	0
c_2	3.38(15)	-1.10	-3.1	-1.78	-0.05
c_3	-4.59(9)	0.89	-5.2	2.76	0.06
c_4	3.31(13)	-2.59	-1.3	-1.37	-0.12
d_{1+2}	5.40(5)	1.75	3.1	-2.20	0.04
d_3	-4.60(7)	-1.36	3.4	1.36	-0.04
d_4	-4.3(1.5)	-	-	$-0.76 \pm 3.71 \pm 0.26 \mp 0.26$	$-0.04 \pm 0.18 \pm 0.03 \pm 0.17$
d_5	-0.37(4)	-0.55	0.7	0.35	0
d_{10}	-31.9(2.6)	-18.6	1.7	$-9.08 \pm 5.50 \pm 3.06 \pm 2.55$	$-0.24 \pm 2.14 \pm 0.18 \mp 0.70 \pm 0.70$
d_{11}	20.5(3.9)	7.01	2.9	$3.03 \mp 4.34 \mp 1.02 \mp 0.51$	$0.16 \mp 0.71 \mp 0.12 \mp 0.70$
d_{12}	34.0(2.7)	16.8	2.0	$5.81 \mp 4.47 \mp 1.96 \mp 1.76$	$0.14 \mp 1.50 \mp 0.15 \mp 0.70 \mp 0.55$
d_{13}	-24.2(3.7)	-6.41	3.8	$-2.30 \pm 3.52 \pm 0.78 \pm 0.57$	$-0.09 \pm 0.68 \pm 0.12 \pm 0.55$
d_{14-15}	-9.88(7)	-1.31	7.6	3.57	-0.12
d_{16}	0.82(80)	-3.95	-0.2	0	-1.40
e_{10}	-22.8(6.3)	22.2	-1.0	$1.65 \mp 10.99 \mp 0.23 \pm 0.49$	$-0.14 \pm 0.20 \pm 0.12 \pm 0.35$
e_{11}	3.6(5.4)	-1.41	-2.6	$-1.07 \mp 0.97 \pm 0.13 \mp 0.13$	$-0.05 \pm 0.17 \pm 0.03 \pm 0.21$
e_{12}	23.5(3.9)	-30.7	-0.8	$-1.22 \pm 10.21 \pm 0.18 \mp 0.18$	$0.16 \mp 0.19 \mp 0.13 \mp 0.48$
e_{13}	-19.8(6.4)	35.4	-0.6	$0.82 \mp 8.82 \mp 0.22 \pm 0.22$	$-0.07 \pm 0.14 \pm 0.08 \pm 0.22$
e_{14}	-0.58(24)	-1.88	0.3	0.46	0
e_{15}	-7.48(45)	-2.69	2.8	2.83	0
e_{16}	2.22(36)	4.48	0.5	-2.00	-0.01
e_{17}	-0.83(32)	-0.29	2.8	-0.37	-0.02
e_{18}	3.49(44)	7.23	0.5	-1.27	-0.05
e_{34}	3.8(21.6)	-1.83	-2.1	$0.59 \pm 1.07 \mp 0.09 \pm 0.09$	$0.06 \mp 0.09 \mp 0.05 \mp 0.28$

TABLE V: LECs determined from fits at order Q^4 in the covariant approach with the additional constraints from the reaction $\pi N \to \pi\pi N$ along with the RG-quantities Δx and $\overline{\Delta x}$ defined in Eq. (18). x_Δ and x_R denote the saturations of the LECs by the Δ and Roper resonances, respectively, using $h_A = 1.35$, $g_1 = \pm 2.29$, $g_{RN} = 0.35$, $b_i = g_{R\Delta} = g_{RR} = c^R_i = \pm 1$. The values of the πN LECs at orders Q^2, Q^3, Q^4 are given in units of GeV^{-1}, GeV^{-2} and GeV^{-3}, respectively.

Q^4	πN	πN+RS	πN+$\pi\pi$N	RS
$d_{00}^+[M_\pi^{-1}]$	-0.37(12)(46)	-1.60(3)(3)	-0.61(10)(40)	-1.36(3)
$d_{10}^+[M_\pi^{-3}]$	-0.86(20)(71)	1.14(6)(13)	-0.51(17)(63)	1.16(2)
$d_{01}^+[M_\pi^{-3}]$	0.79(4)(22)	0.92(3)(18)	0.76(4)(23)	1.16(2)
$d_{20}^+[M_\pi^{-5}]$	1.29(9)(25)	0.39(3)(4)	1.14(8)(21)	0.196(3)
$d_{11}^+[M_\pi^{-5}]$	0.64(4)(13)	0.42(3)(8)	0.64(4)(13)	0.185(3)
$d_{02}^+[M_\pi^{-5}]$	0.033(7)(2)	0.001(6)(8)	0.032(7)(2)	0.0336(6)
$b_{00}^+[M_\pi^{-3}]$	-5.2(2)(1.1)	-4.7(1)(1.3)	-5.4(2)(1.1)	-3.45(7)
$d_{00}^-[M_\pi^{-2}]$	1.15(2)(15)	1.39(1)(2)	1.23(2)(13)	1.41(1)
$d_{10}^-[M_\pi^{-4}]$	0.30(3)(23)	-0.10(2)(7)	0.16(3)(20)	-0.159(4)
$d_{01}^-[M_\pi^{-4}]$	-0.210(4)(33)	-0.22(0)(2)	-0.21(0)(3)	-0.141(5)
$b_{00}^-[M_\pi^{-2}]$	6.4(7)(2.1)	10.4(4)(5)	5.8(7)(2.2)	10.49(11)
$b_{10}^-[M_\pi^{-4}]$	5.8(5)(1.1)	3.1(3)(5)	6.2(5)(1.2)	1.00(3)
$b_{01}^-[M_\pi^{-4}]$	0.38(16)(4)	-0.09(14)(7)	0.43(16)(5)	0.21(2)
$d_{00}^+[M_\pi^{-1}]$	-0.48(12)(22)	-1.69(3)(7)	-0.50(10)(22)	-1.36(3)
$d_{10}^+[M_\pi^{-3}]$	-0.67(20)(46)	1.17(5)(4)	-0.68(17)(46)	1.16(2)
$d_{01}^+[M_\pi^{-3}]$	0.70(4)(20)	0.73(3)(18)	0.63(4)(21)	1.16(2)
$d_{20}^+[M_\pi^{-5}]$	1.30(9)(25)	0.45(2)(5)	1.31(8)(25)	0.196(3)
$d_{11}^+[M_\pi^{-5}]$	0.80(4)(17)	0.54(3)(11)	0.85(4)(18)	0.185(3)
$d_{02}^+[M_\pi^{-5}]$	0.052(8)(4)	-0.06(1)(2)	0.055(8)(5)	0.0336(6)
$b_{00}^+[M_\pi^{-3}]$	-1.44(21)(2.04)	-3.0(2)(1.5)	-2.0(2)(1.9)	-3.45(7)
$d_{00}^-[M_\pi^{-2}]$	0.71(2)(24)	1.27(2)(7)	0.79(2)(22)	1.41(1)
$d_{10}^-[M_\pi^{-4}]$	0.77(3)(34)	-0.08(3)(10)	0.66(3)(31)	-0.159(4)
$d_{01}^-[M_\pi^{-4}]$	-0.060(4)(89)	-0.11(0)(7)	-0.07(0)(9)	-0.141(5)
$b_{00}^-[M_\pi^{-2}]$	6.7(8)(1.3)	10.1(5)(6)	4.9(7)(1.7)	10.49(11)
$b_{10}^-[M_\pi^{-4}]$	6.3(5)(1.2)	3.6(3)(6)	7.4(5)(1.5)	1.00(3)
$b_{01}^-[M_\pi^{-4}]$	0.47(16)(6)	-0.96(14)(27)	0.57(16)(9)	0.21(2)
$d_{00}^+[M_\pi^{-1}]$	-1.22(9)(12)	-1.46(3)(2)	-1.12(8)(14)	-1.36(3)
$d_{10}^+[M_\pi^{-3}]$	0.75(11)(25)	1.14(4)(13)	0.63(11)(28)	1.16(2)
$d_{01}^+[M_\pi^{-3}]$	0.97(3)(16)	1.10(3)(13)	0.97(3)(17)	1.16(2)
$d_{20}^+[M_\pi^{-5}]$	0.54(4)(11)	0.40(2)(8)	0.58(4)(12)	0.196(3)
$d_{11}^+[M_\pi^{-5}]$	0.43(2)(9)	0.34(2)(7)	0.44(2)(10)	0.185(3)
$d_{02}^+[M_\pi^{-5}]$	-0.004(6)(5)	-0.012(5)(7)	-0.002(6)(5)	0.0336(6)
$b_{00}^+[M_\pi^{-3}]$	-6.05(10)(0.45)	-5.6(1)(6)	-6.10(9)(43)	-3.45(7)
$d_{00}^-[M_\pi^{-2}]$	1.40(1)(3)	1.37(1)(3)	1.41(1)(3)	1.41(1)
$d_{10}^-[M_\pi^{-4}]$	-0.21(1)(5)	-0.18(1)(5)	-0.21(1)(5)	-0.159(4)
$d_{01}^-[M_\pi^{-4}]$	-0.247(3)(23)	-0.24(0)(2)	-0.25(0)(2)	-0.141(5)
$b_{00}^-[M_\pi^{-2}]$	8.0(5)(1.3)	10.4(4)(7)	7.6(5)(1.5)	10.49(11)
$b_{10}^-[M_\pi^{-4}]$	4.13(27)(88)	3.2(2)(7)	4.31(27)(92)	1.00(3)
$b_{01}^-[M_\pi^{-4}]$	0.38(11)(7)	0.44(10)(9)	0.36(11)(7)	0.21(2)

TABLE VI: Subthreshold parameters at order Q^4 in comparison with the RS analysis values. The upper/middle/lower table refer to results in the HB-NN, HB-πN and covariant counting, respectively. The statistical and theoretical uncertainties are given in the first and second bracket, respectively.

Q^4	πN	πN+RS	πN+$\pi\pi$N	RS
$a_{0+}^{+}[M_\pi^{-1}]$	3.1(9)(10)	-6.2(5)(4.5)	0.2(7)(1.1)	-0.9(1.4)
$a_{0+}^{-}[M_\pi^{-1}]$	82.8(3)(5)	83.7(2)(1.6)	82.9(3)(5)	85.4(9)
$a_{1+}^{+}[M_\pi^{-3}]$	136.0(5)(3.9)	137.0(4)(3.2)	135.8(5)(3.9)	131.2(1.7)
$a_{1+}^{-}[M_\pi^{-3}]$	-83.9(5)(2.1)	-87.0(4)(7)	-83.6(5)(2.2)	-80.3(1.1)
$a_{1-}^{+}[M_\pi^{-3}]$	-57.9(7)(3.2)	-56.2(5)(3.1)	-58.7(7)(3.3)	-50.9(1.9)
$a_{1-}^{+}[M_\pi^{-3}]$	-11.9(1.3)(1.9)	-6.2(8)(1.7)	-13.0(1.2)(2.0)	-9.9(1.2)
$b_{0+}^{+}[M_\pi^{-3}]$	-53.5(3.5)(4.1)	-14.4(1.6)(16.4)	-42.7(2.6)(4.7)	-45.0(1.0)
$b_{0+}^{-}[M_\pi^{-3}]$	17.5(4)(1.2)	15.1(4)(4.0)	17.4(5)(1.2)	4.9(8)
$a_{0+}^{+}[M_\pi^{-1}]$	2.9(9)(8)	-12.1(6)(4.1)	1.3(7)(1.2)	-0.9(1.4)
$a_{0+}^{-}[M_\pi^{-1}]$	82.2(3)(2)	85.4(3)(1.3)	82.4(3)(3)	85.4(9)
$a_{1+}^{+}[M_\pi^{-3}]$	133.1(5)(4.5)	129.6(4)(4.6)	132.6(5)(4.6)	131.2(1.7)
$a_{1+}^{-}[M_\pi^{-3}]$	-82.7(5)(2.2)	-85.6(4)(9)	-81.6(5)(2.5)	-80.3(1.1)
$a_{1-}^{+}[M_\pi^{-3}]$	-54.1(7)(2.5)	-63.1(6)(2.9)	-55.9(7)(2.6)	-50.9(1.9)
$a_{1-}^{+}[M_\pi^{-3}]$	-10.9(1.3)(2.3)	-10.0(8)(1.8)	-14.1(1.2)(2.6)	-9.9(1.2)
$b_{0+}^{+}[M_\pi^{-3}]$	-52.7(3.5)(2.9)	6.0(2.0)(16.5)	-47.9(2.7)(4.0)	-45.0(1.0)
$b_{0+}^{-}[M_\pi^{-3}]$	22.4(5)(3)	14.9(4)(2.4)	22.1(4)(2)	4.9(8)
$a_{0+}^{+}[M_\pi^{-1}]$	0.0(9)(1.7)	0.0(5)(2.4)	0.7(8)(1.5)	-0.9(1.4)
$a_{0+}^{-}[M_\pi^{-1}]$	83.3(3)(5)	83.2(2)(5)	83.5(3)(5)	85.4(9)
$a_{1+}^{+}[M_\pi^{-3}]$	135.8(5)(3.5)	137.4(5)(3.0)	135.6(5)(3.5)	131.2(1.7)
$a_{1+}^{-}[M_\pi^{-3}]$	-84.3(5)(1.6)	-86.4(4)(1.0)	-83.9(5)(1.7)	-80.3(1.1)
$a_{1-}^{+}[M_\pi^{-3}]$	-59.6(7)(3.0)	-56.2(6)(2.8)	-60.0(6)(3.1)	-50.9(1.9)
$a_{1-}^{+}[M_\pi^{-3}]$	-13.6(1.2)(2.5)	-7.7(9)(2.2)	-14.8(1.1)(2.6)	-9.9(1.2)
$b_{0+}^{+}[M_\pi^{-3}]$	-37.8(3.5)(6.9)	-35.3(2.0)(9.4)	-41.1(3.2)(6.2)	-45.0(1.0)
$b_{0+}^{-}[M_\pi^{-3}]$	16.3(6)(1.6)	15.8(5)(1.9)	16.0(6)(1.7)	4.9(8)

TABLE VII: Threshold parameters at order Q^4 in comparison with RS analysis values. The upper/middle/lower table refer to results in the HB-NN, HB-πN and covariant counting, respectively. The statistical and theoretical uncertainties are given in the first and second bracket, respectively.
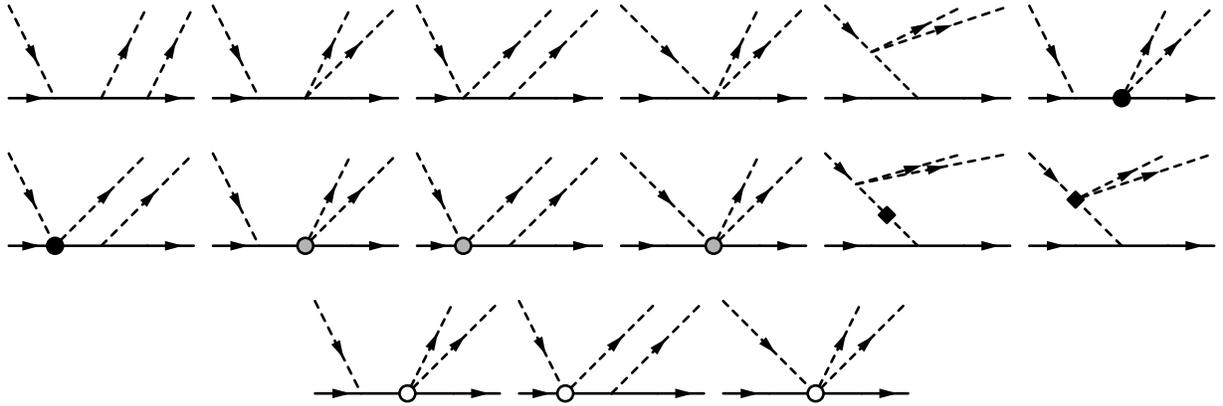
FIG. 1: Tree-level graphs contributing to the reaction $\pi N \to \pi\pi N$. The black/gray/white blobs denote insertions of the $c_i/d_i/e_i$- vertices, whereas the black diamonds denote insertions of the l_i vertices. Dashed and solid lines refer to pions and nucleons, respectively. Crossed diagrams are not shown.
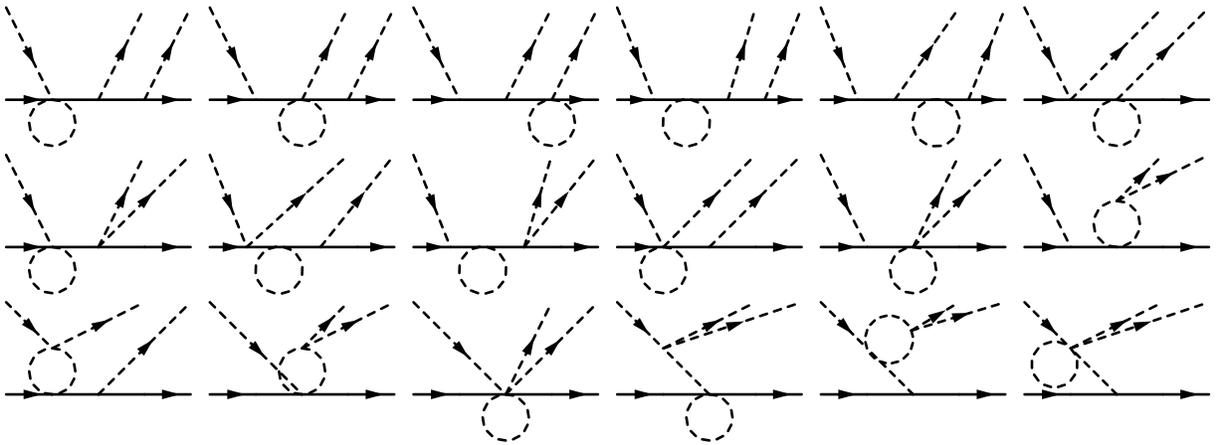
FIG. 2: One-loop graphs of the tadpole type contributing to the reaction $\pi N \to \pi\pi N$. For notation see Fig. 1.
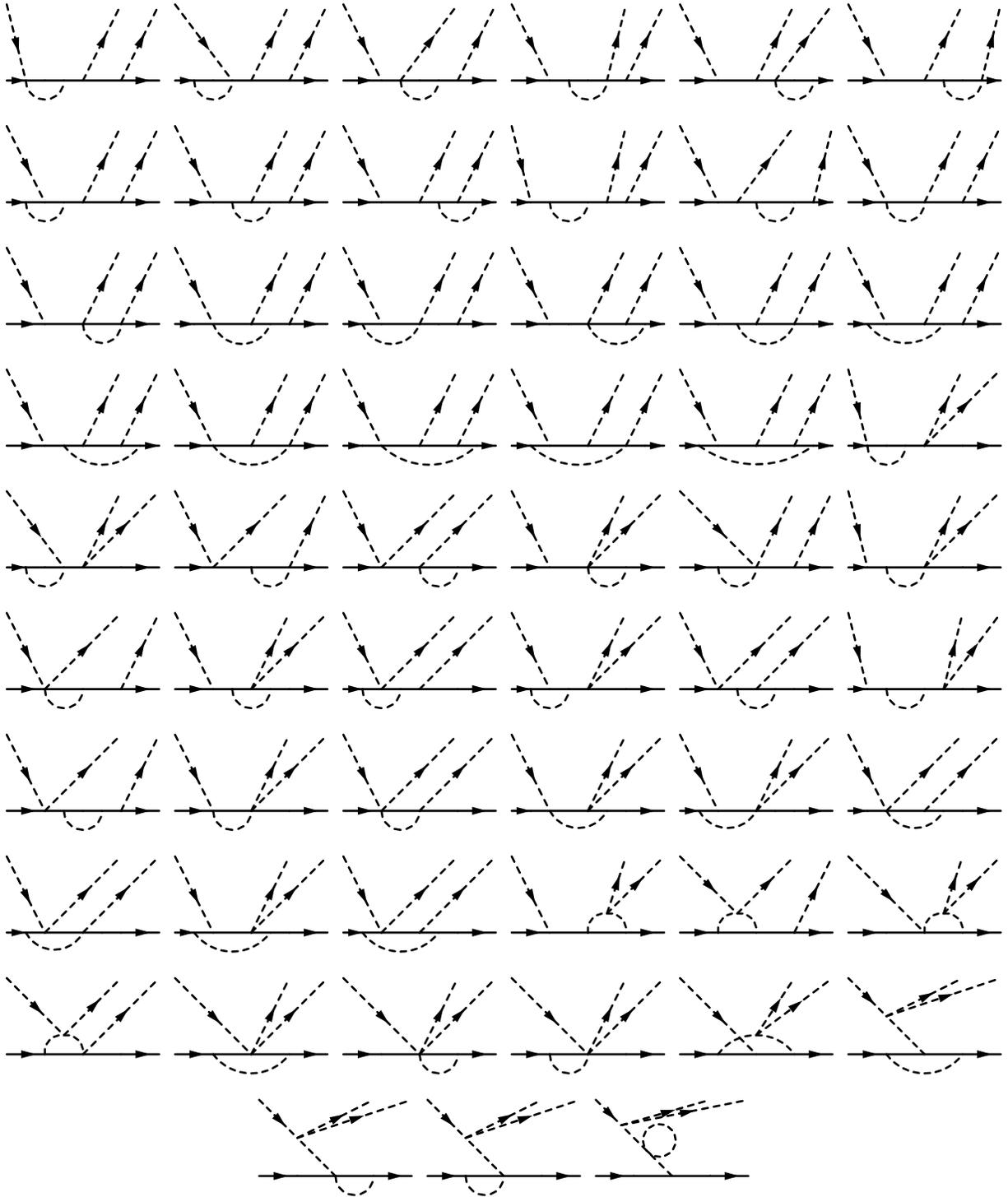
FIG. 3: One-loop graphs of the self-energy type contributing to the reaction $\pi N \to \pi\pi N$. For notation see Fig. 1.
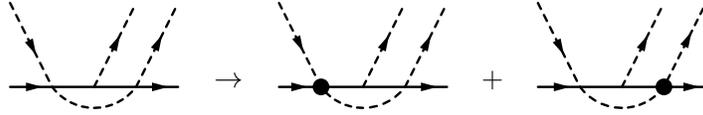
FIG. 4: Transition from leading to next-to-leading order loop graphs. For notation see Fig. 1.
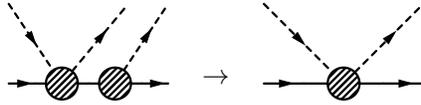
FIG. 5: Transition from $\pi N \to \pi\pi N$ graphs to $\pi N \to \pi N$ graphs. The shaded blob denotes any possible interaction. For notation see Fig. 1.

FIG. 6: Leading-order Δ pole diagrams, where the double solid line refers to the Δ. For notation see Fig. 1.
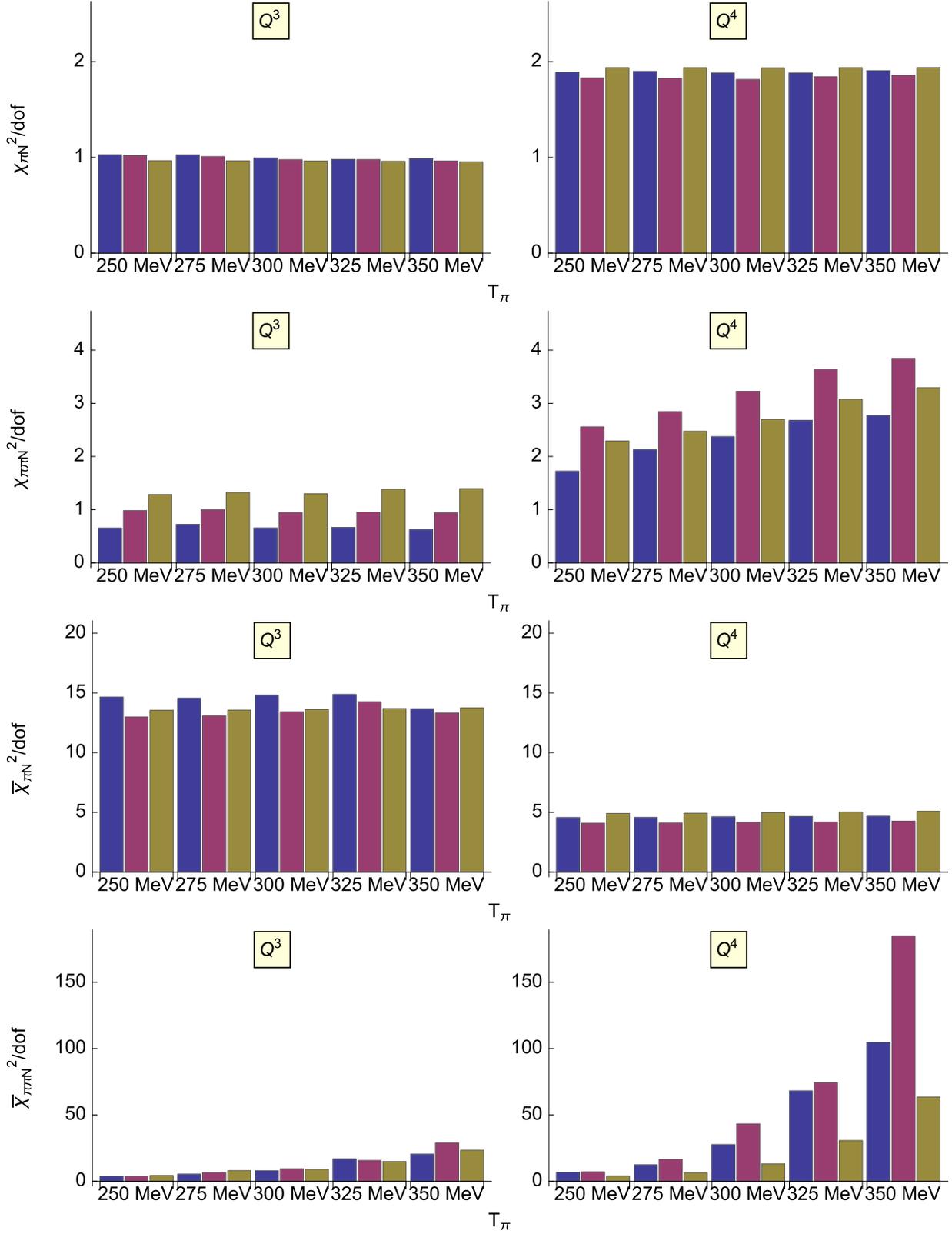
FIG. 7: Reduced $\chi^2_{\pi N}/\chi^2_{\pi\pi N}$ (with theoretical error) and $\bar{\chi}^2_{\pi N}/\bar{\chi}^2_{\pi\pi N}$ (without theoretical error) for fits up to various maximum energies $T_{\pi,\pi\pi N}$. The blue/red/green bars denote the results for the HB-NN/HB-πN/Cov counting.
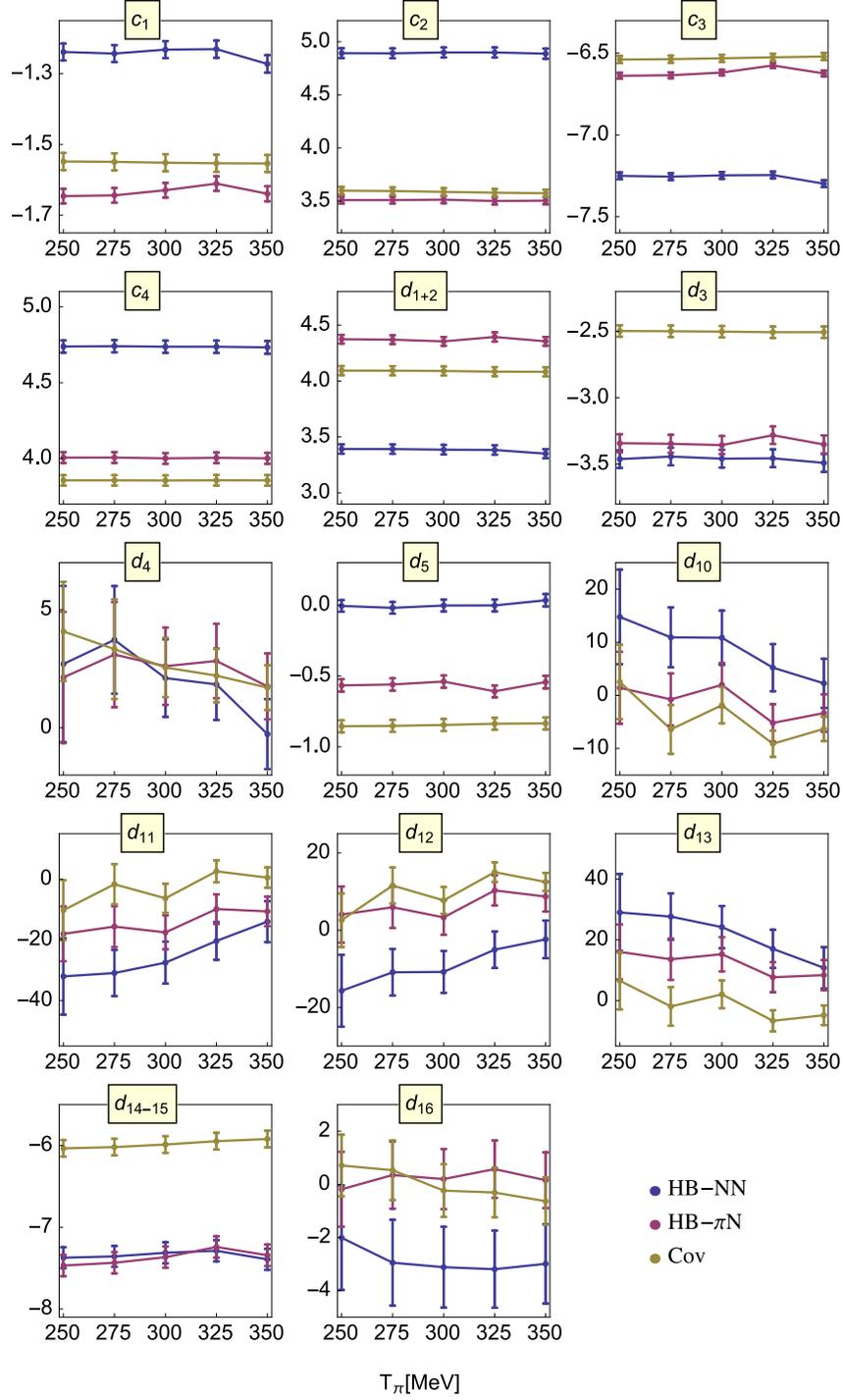
FIG. 8: Change of the LECs at Q^3 over the maximum fit energy $T_{\pi,\pi\pi N}$.
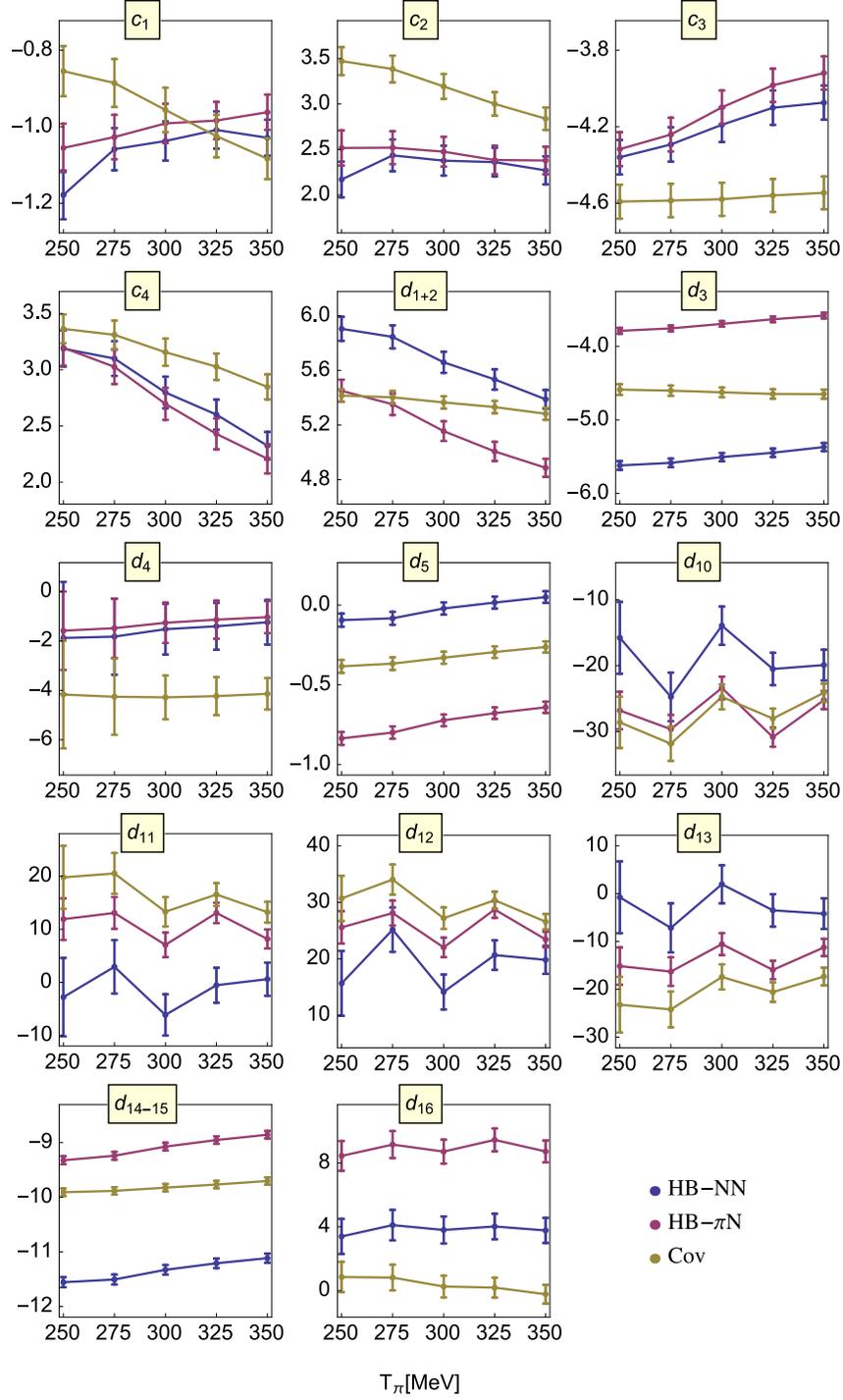
FIG. 9: Change of the LECs at Q^4 over the maximum fit energy $T_{\pi,\pi\pi N}$.
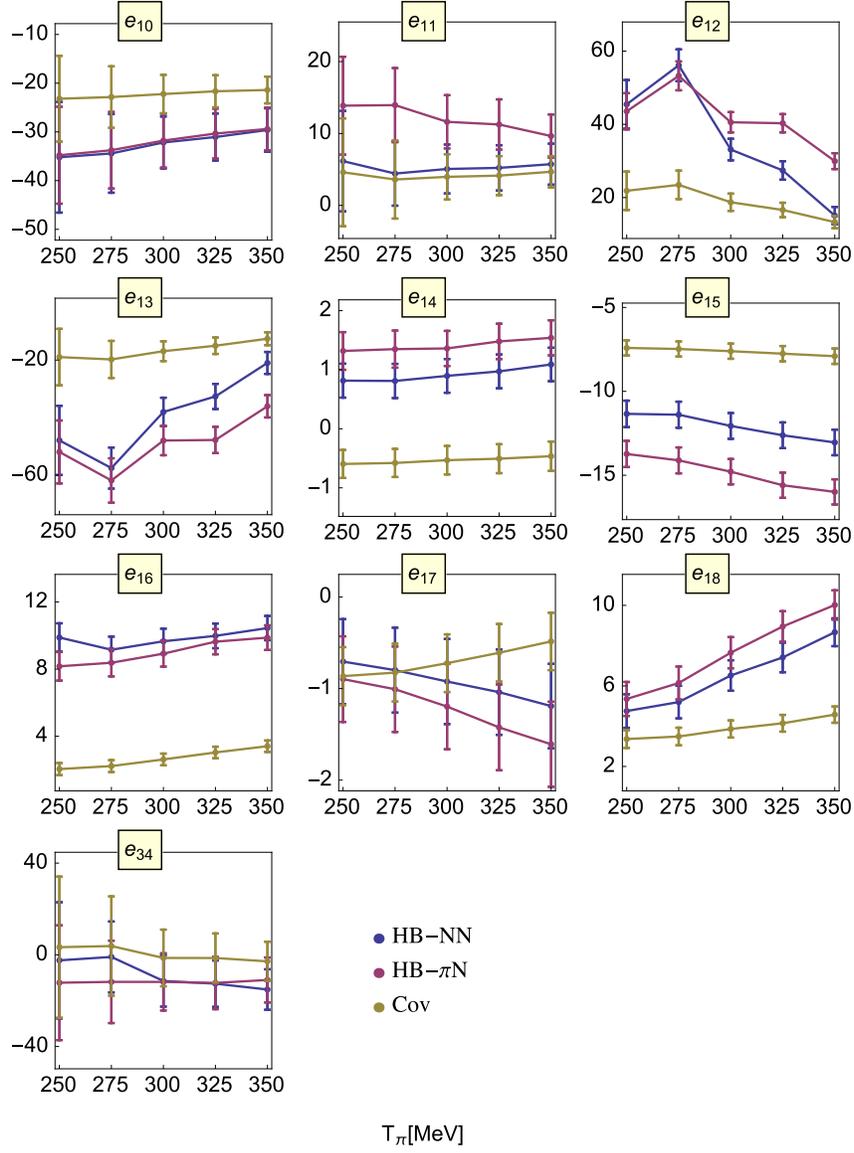
FIG. 10: Change of the LECs at Q^4 over the maximum fit energy $T_{\pi,\pi\pi N}$.
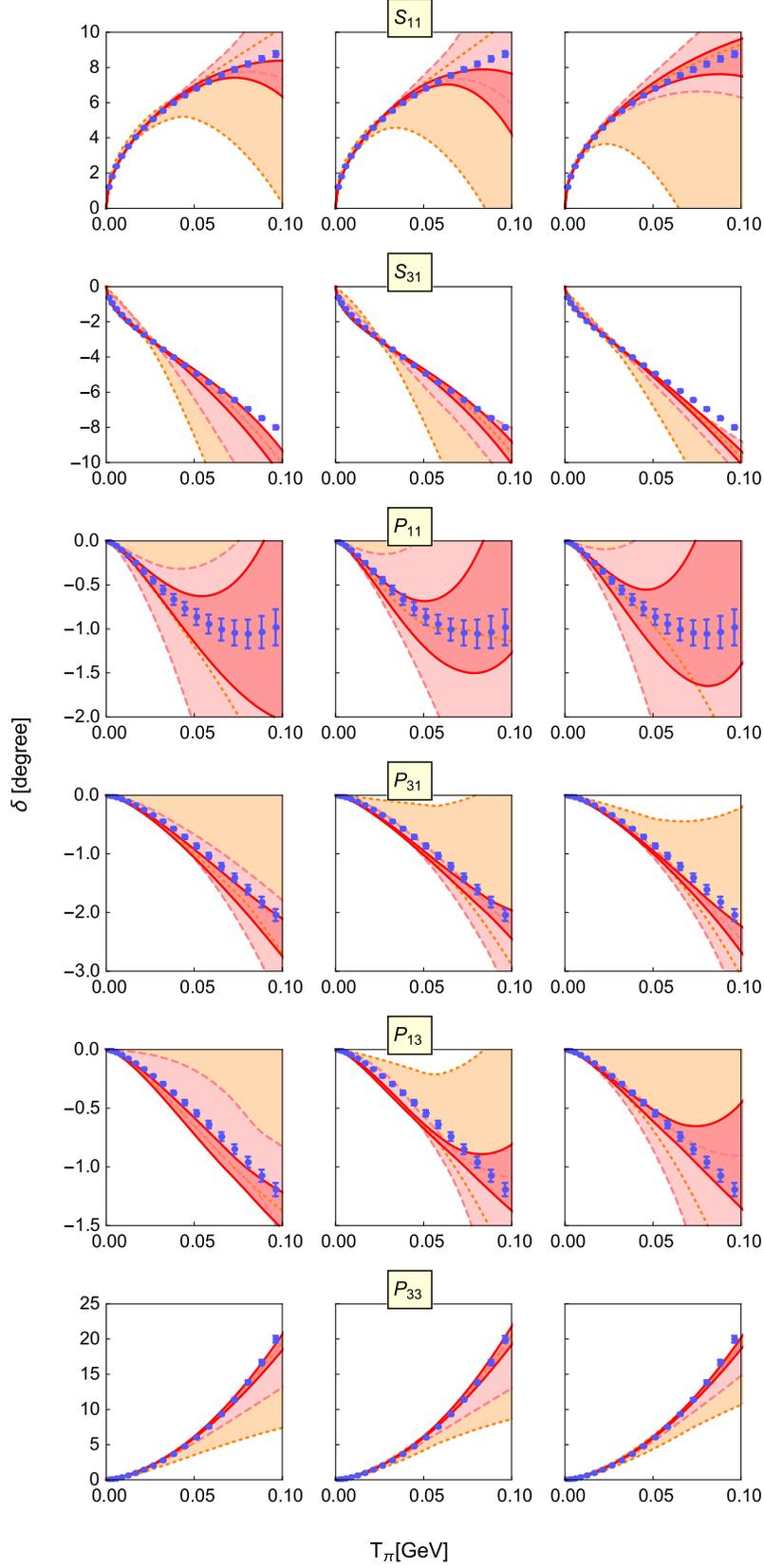
FIG. 11: Predictions for the $\pi N \to \pi N$ S and P waves up to $T_\pi = 100$ MeV with the LECs in Table I taken as input. Columns from left to right correspond to the predictions in the HB-NN, HB-πN and covariant counting, respectively. The orange, pink and red (dotted, dashed and solid) bands refer to the Q^2, Q^3 and Q^4 results including theoretical uncertainties, respectively.
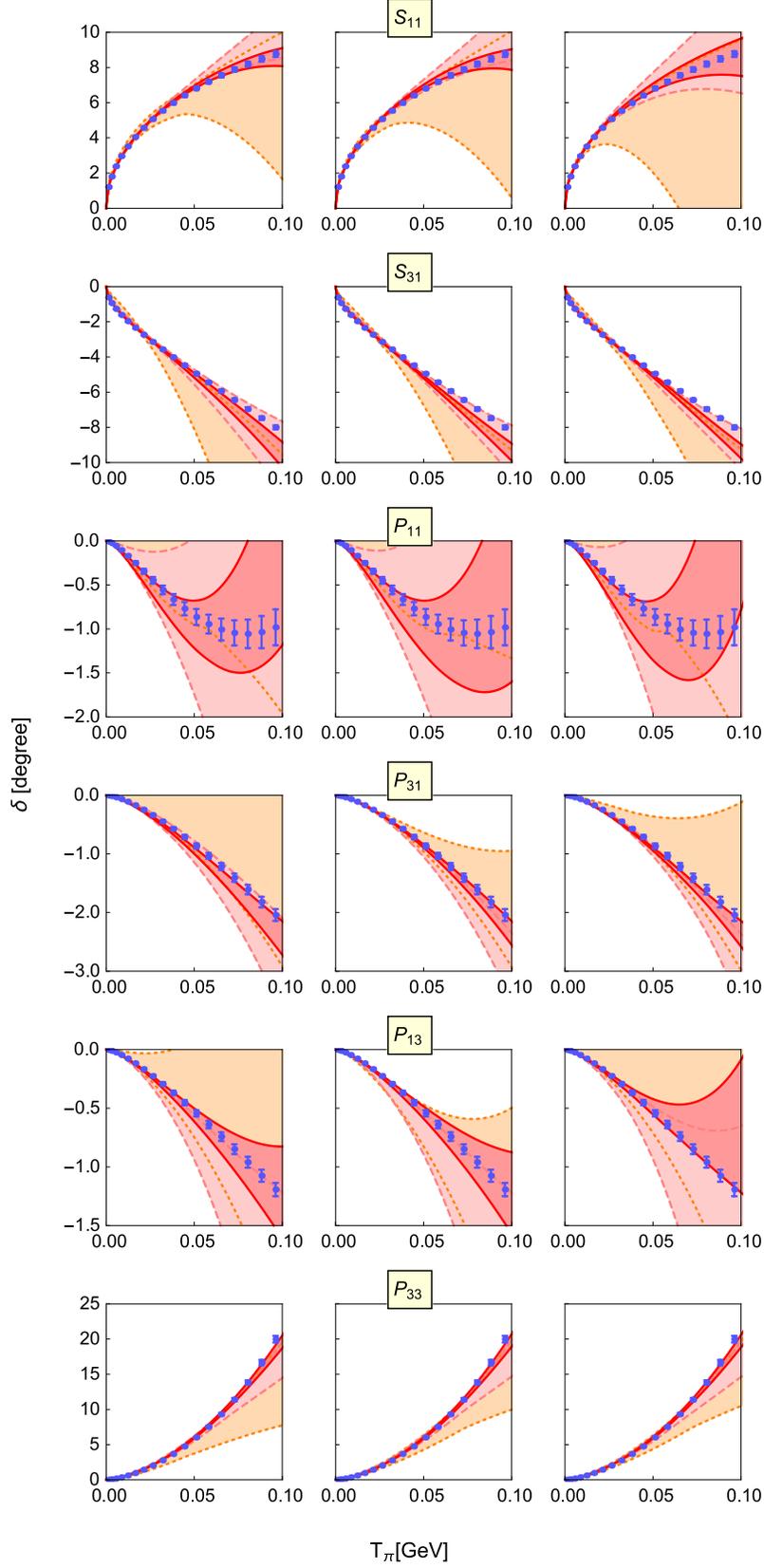
FIG. 12: Predictions for the $\pi N \to \pi N$ S and P waves up to $T_\pi = 100$ MeV with the LECs in Tables II and III taken as input. Columns from left to right correspond to the predictions in the HB-NN, HB-πN and covariant counting, respectively. The orange, pink and red (dotted, dashed and solid) bands refer to the Q^2, Q^3 and Q^4 results including theoretical uncertainties, respectively.
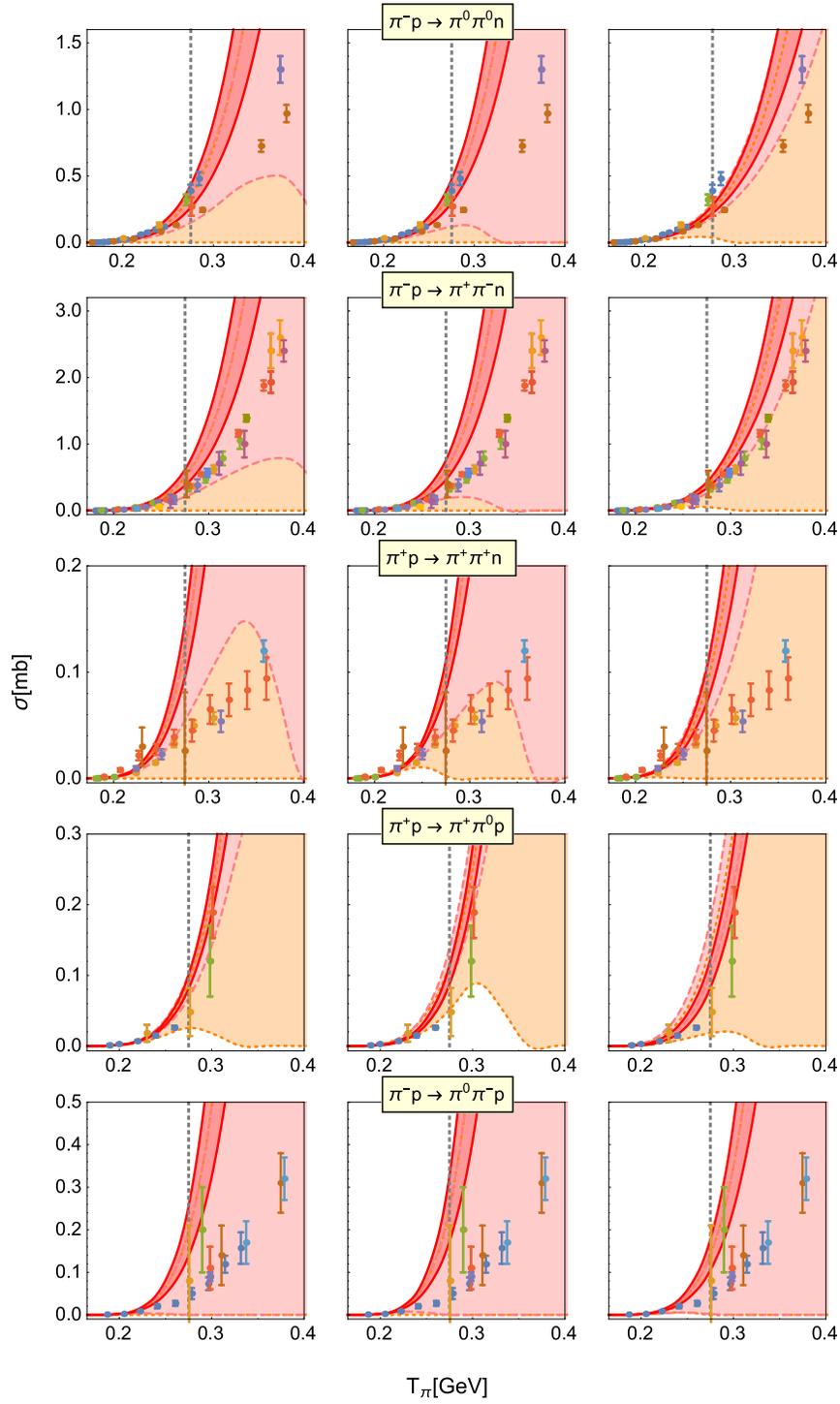
FIG. 13: Predictions for the $\pi N \to \pi\pi N$ total cross sections up to $T_\pi = 400$ MeV. The energies used in the fit are on the left of the vertical dotted lines. For remaining notation see the caption of Fig. 12.
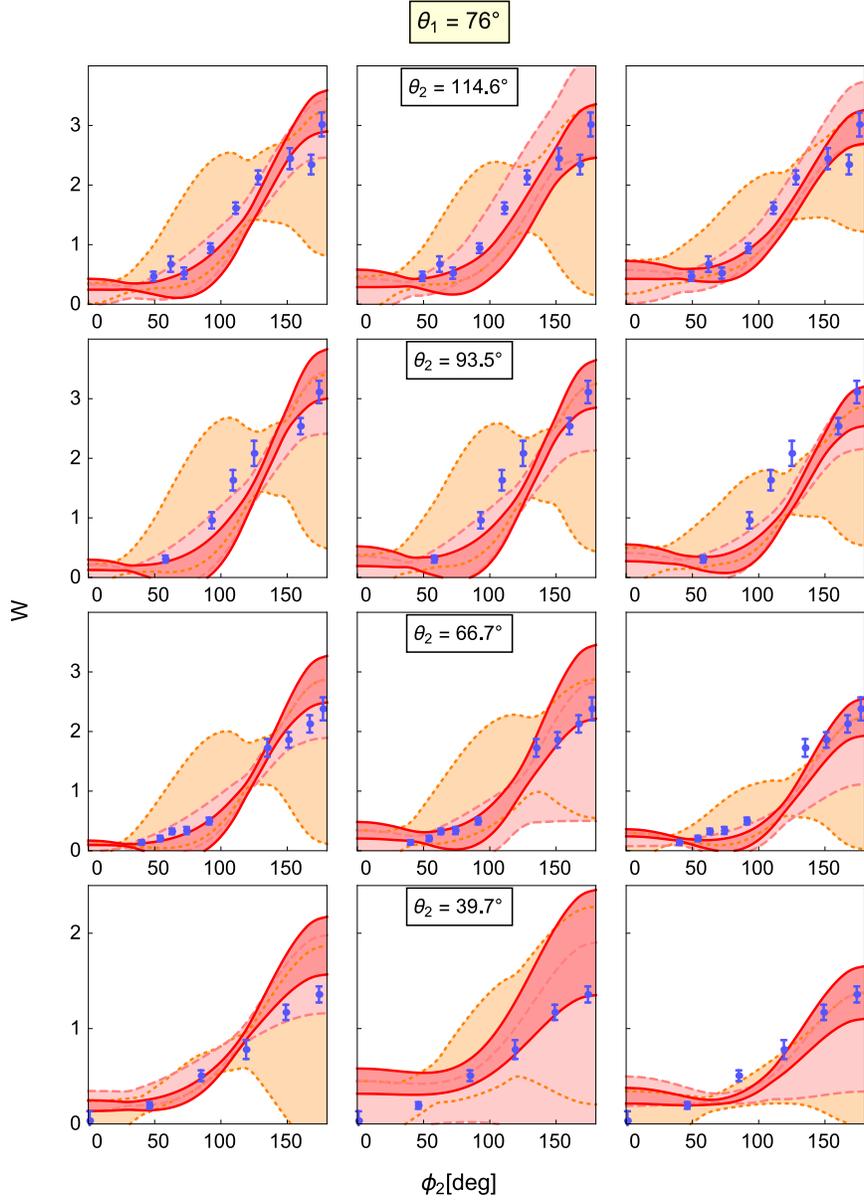
FIG. 14: Predictions for the angular correlation functions in the $\pi^- p \to \pi^+ \pi^- n$ channel at fixed θ_1 and θ_2 for $T_\pi = 280$ MeV. The lower/middle/upper panel correspond to the HB-NN, HB-πN and covariant counting. The orange, pink and red (dotted, dashed and solid) bands refer to the Q^2, Q^3 and Q^4 results including theoretical uncertainties, respectively.
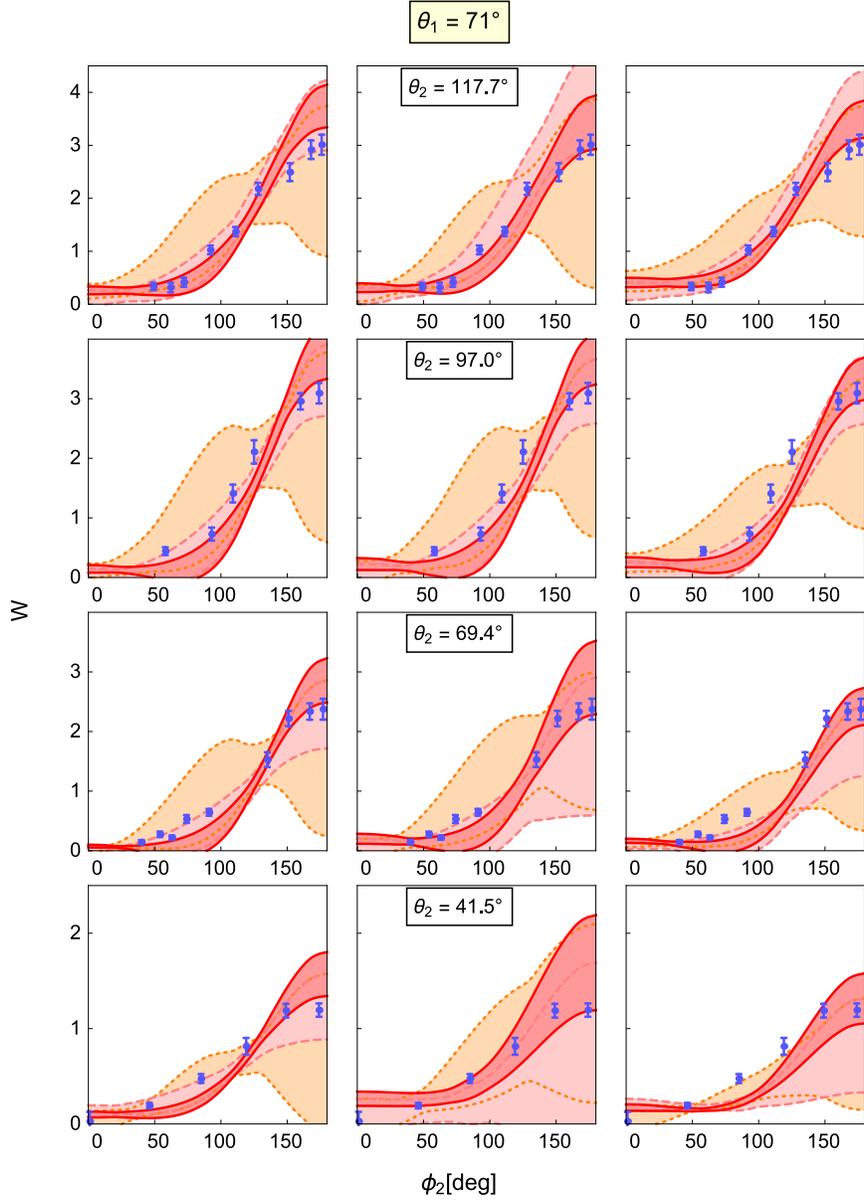
FIG. 15: Predictions for the angular correlation functions in the $\pi^- p \to \pi^+ \pi^- n$ channel at fixed θ_1 and θ_2 for $T_\pi = 280$ MeV. The lower/middle/upper panel correspond to the HB-NN, HB-πN and covariant counting. The orange, pink and red (dotted, dashed and solid) bands refer to the Q^2, Q^3 and Q^4 results including theoretical uncertainties, respectively.
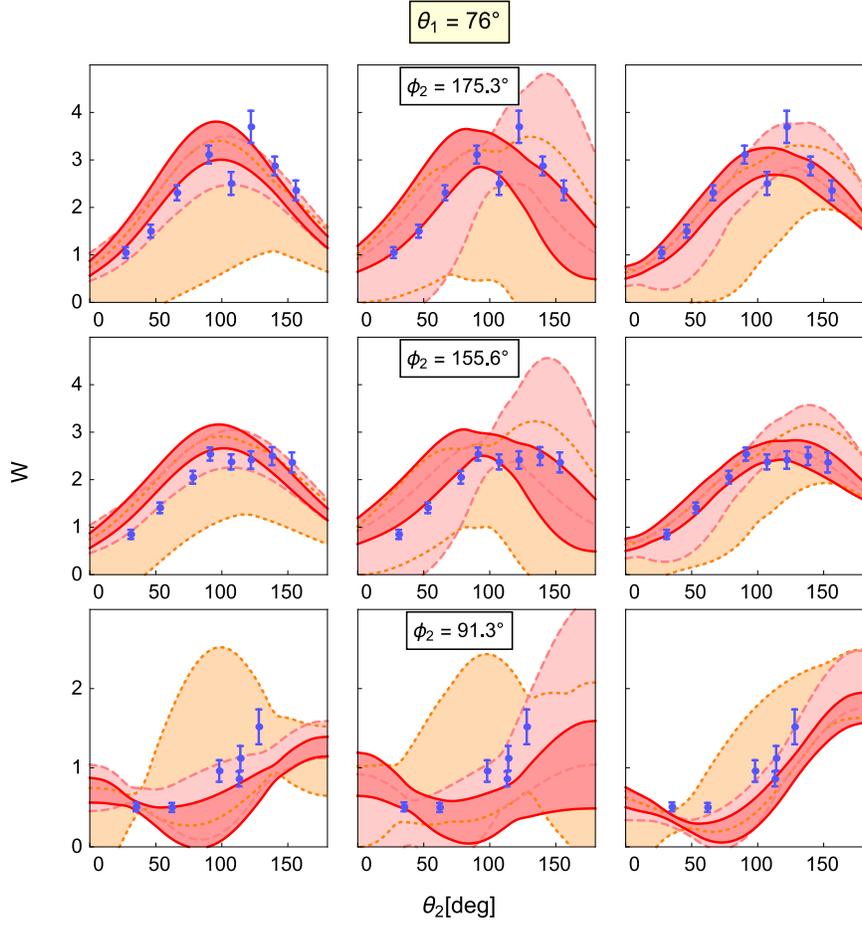
FIG. 16: Predictions for the angular correlation functions in the $\pi^- p \to \pi^+ \pi^- n$ channel at fixed θ_1 and ϕ_2 for $T_\pi = 280$ MeV. For remaining notation see Fig. 14.
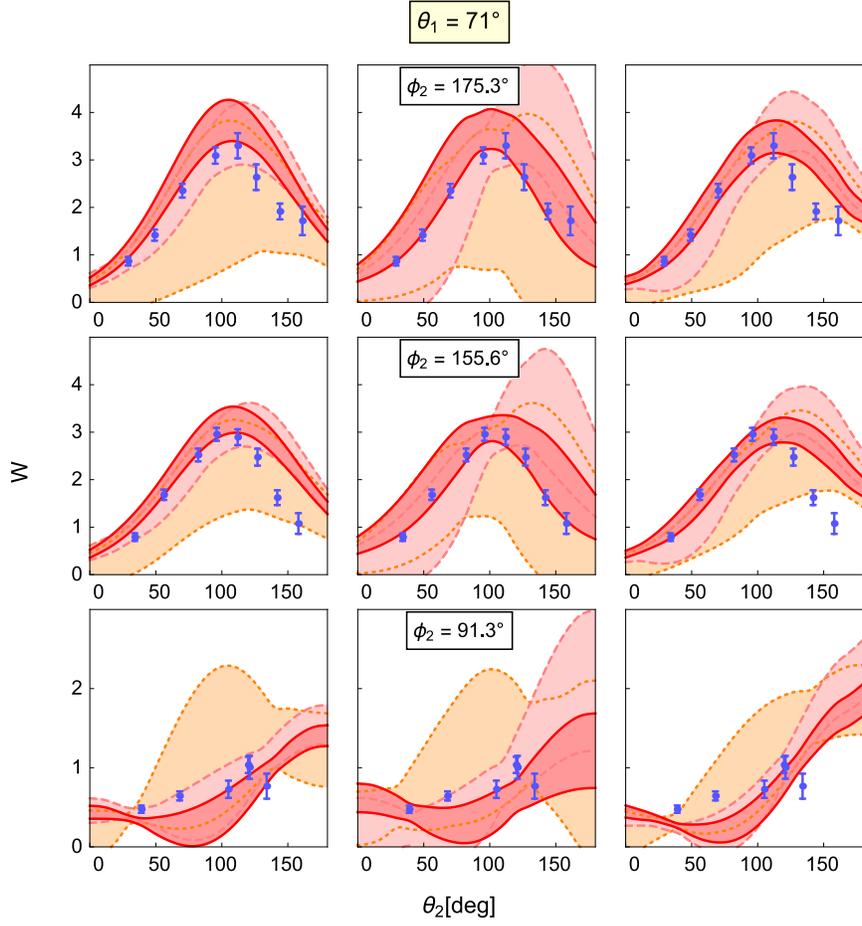
FIG. 17: Predictions for the angular correlation functions in the $\pi^- p \to \pi^+ \pi^- n$ channel at fixed θ_1 and ϕ_2 for $T_\pi = 280$ MeV. For remaining notation see Fig. 14.
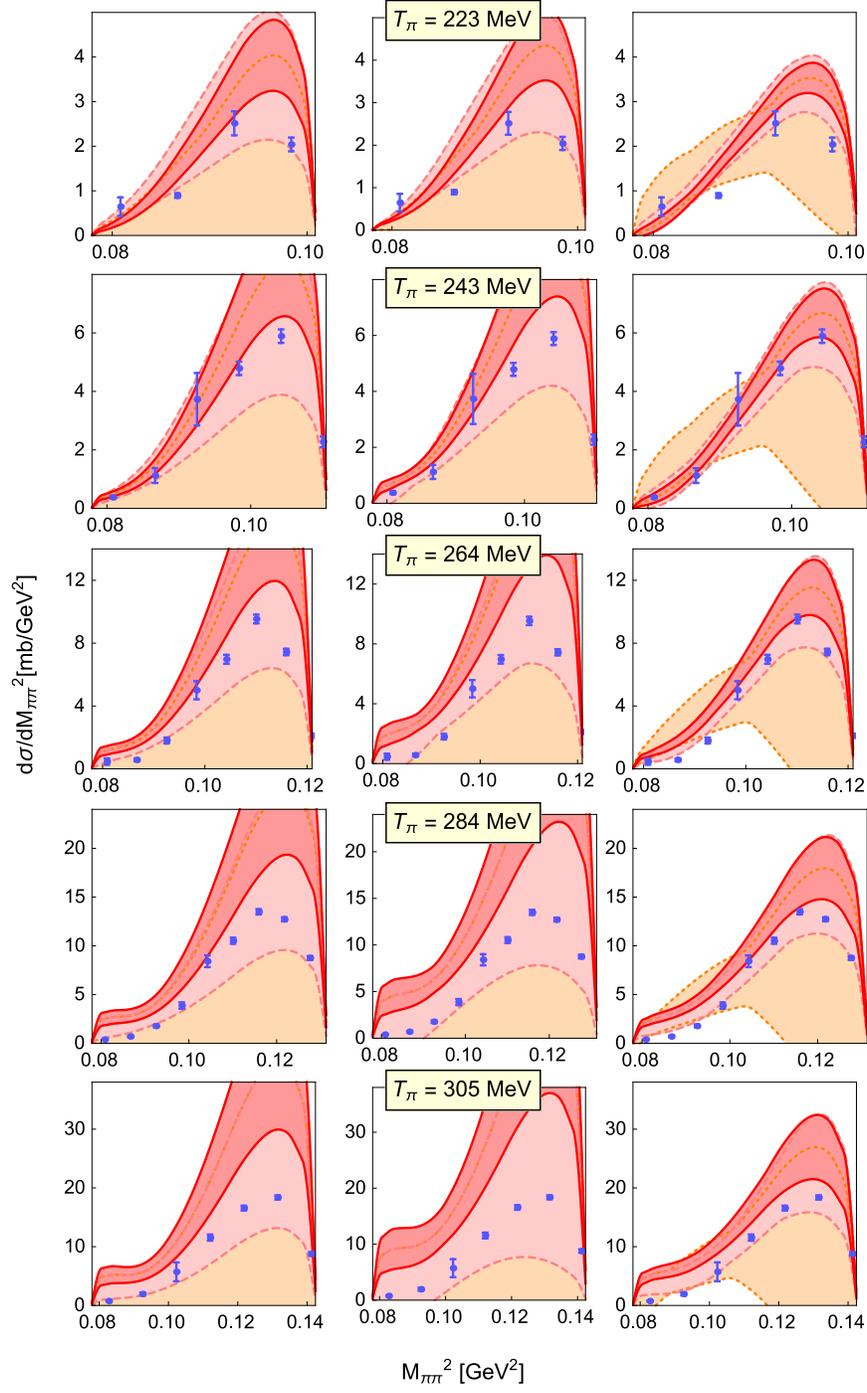
FIG. 18: Predictions for the single-differential cross sections with respect to $M_{\pi\pi}^2$ for the channel $\pi^- p \to \pi^+ \pi^- n$. For remaining notation see Fig. 12.
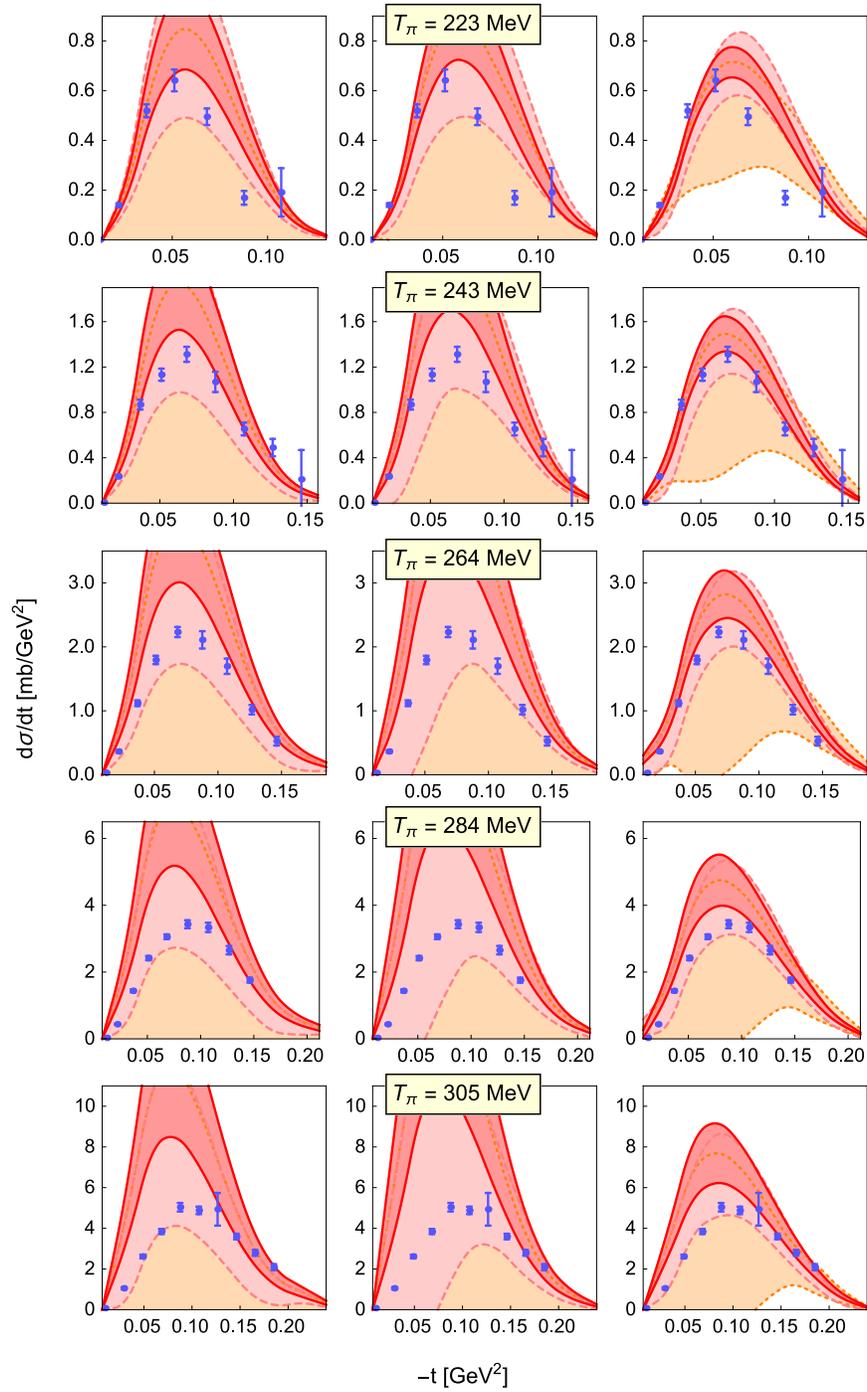
FIG. 19: Predictions for the single-differential cross sections with respect to t for the channel $\pi^- p \to \pi^+ \pi^- n$. For remaining notation see Fig. 12.
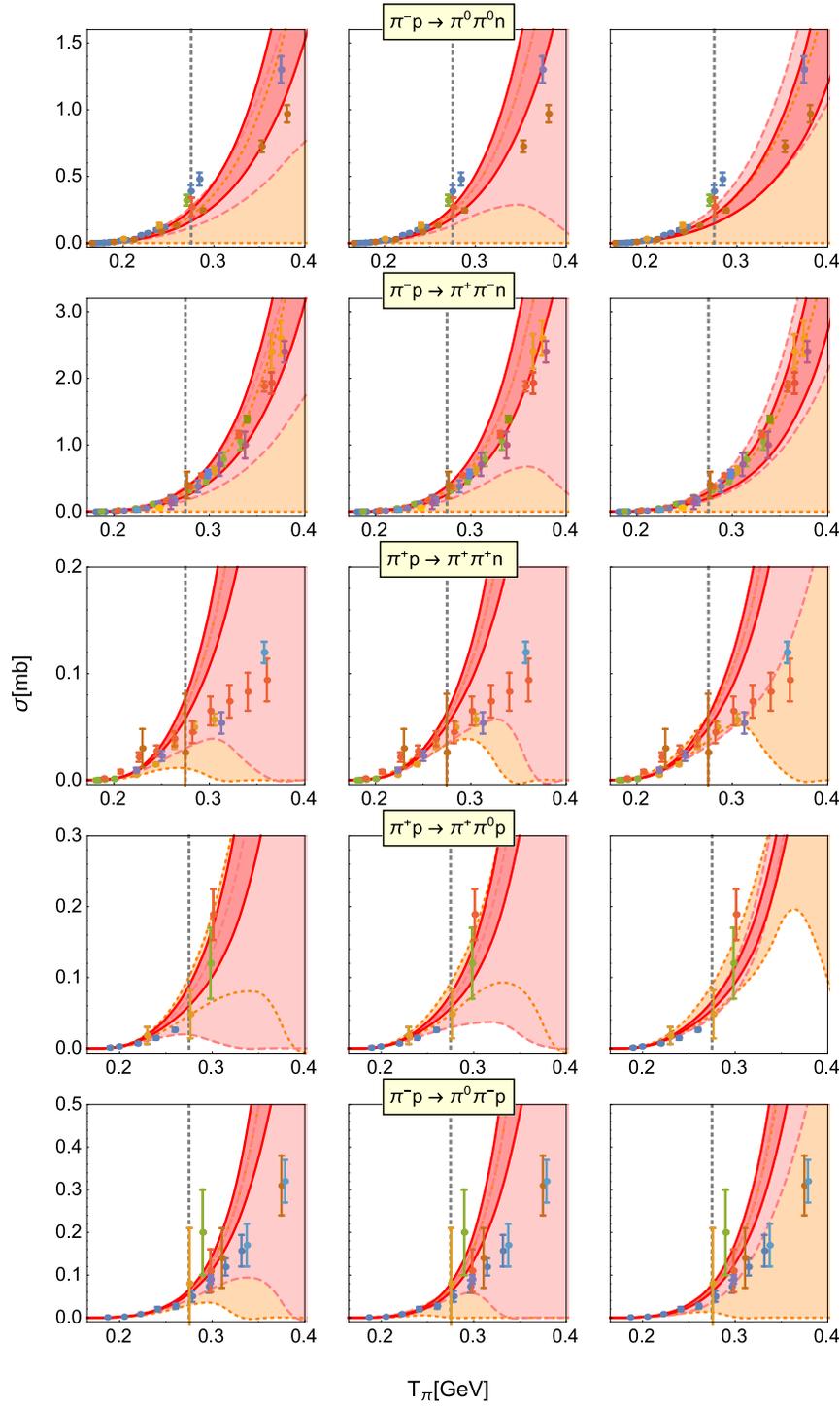
FIG. 20: Predictions for the $\pi N \to \pi \pi N$ total cross sections up to $T_\pi = 400$ MeV. Columns from left to right correspond to the predictions in the HB-NN, HB-πN and covariant counting, respectively. The orange, pink and red (dotted, dashed and solid) bands refer to the $Q^2 + \delta^1$, $Q^3 + \delta^1$ and $Q^4 + \delta^1$ results including theoretical uncertainties, respectively.
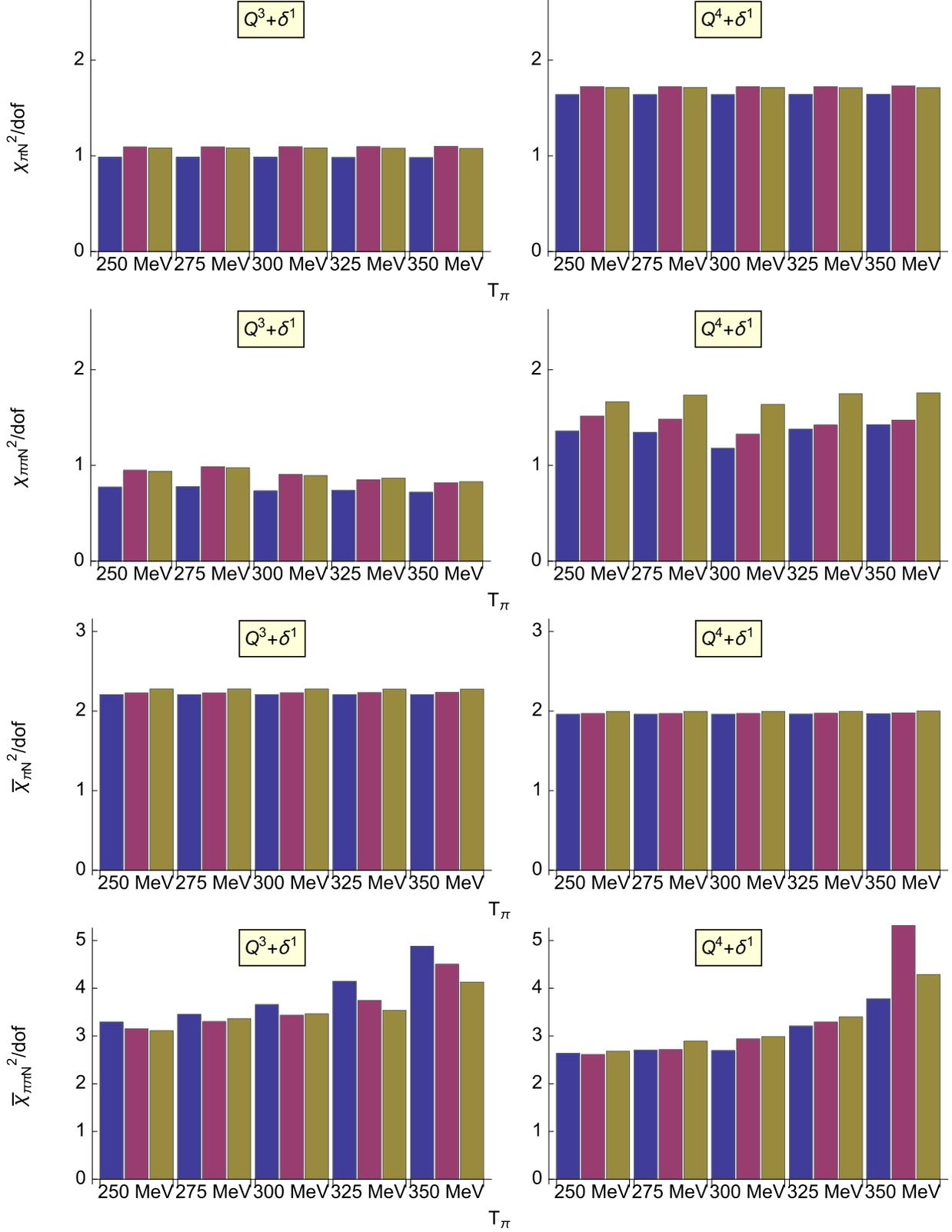
FIG. 21: Reduced $\chi^2_{\pi N}/\chi^2_{\pi\pi N}$ (with theoretical error) and $\bar{\chi}^2_{\pi N}/\bar{\chi}^2_{\pi\pi N}$ (without theoretical error) for fits including leading Δ-pole contributions up to various maximum energy $T_{\pi,\pi\pi N}$. The blue/red/green bars denote the results for the HB-NN/HB-πN/Cov counting.